Article

Geochemistry of REY-Enriched Phosphorites in Zhijin Region, Guizhou Province, SW China: Insight into the Origin of REY

Shan He [1,2], Yong Xia [1,*], Jiafei Xiao [1], Daniel Gregory [3], Zhuojun Xie [1], Qinping Tan [1], Haiying Yang [1,4], Haiyan Guo [1,5], Shengwei Wu [1,2] and Xingxiang Gong [1,6]

[1] State Key Laboratory of Ore Deposit Geochemistry, Institute of Geochemistry, Chinese Academy of Sciences, Guiyang 550081, China; heshan@mail.gyig.ac.cn (S.H.); xiaojiafei@vip.gyig.ac.cn (J.X.); xiezhuojun@vip.gyig.ac.cn (Z.X.); tanqinping@vip.gyig.ac.cn (Q.T.); yanghy527@ynu.edu.cn (H.Y.); xy352748309@163.com (H.G.); wushengwei@mail.gyig.ac.cn (S.W.); gongxingxiang@mail.gyig.ac.cn (X.G.)

[2] University of Chinese Academy of Sciences, Beijing 101408, China

[3] Department of Earth Sciences, University of Toronto, Earth Sciences Centre, 22 Ursula Franklin Street, Toronto, ON M5S 3B1, Canada; daniel.gregory@utoronto.ca

[4] School of Earth Sciences, Yunnan University, Kunming 650500, China

[5] School of Pharmacy, Chengdu University of Traditional Chinese Medicine, Chengdu 611137, China

[6] Reserve Bureau of Land and Mineral Resources of Guizhou Province, Guiyang 550081, China

* Correspondence: xiayong@vip.gyig.ac.cn

Abstract: The rare earth elements and yttrium (REY)-enriched phosphorites in the Zhijin region, southwest China, have attracted much attention, yet its origin has not been sufficiently addressed. The geology, mineralogy and geochemistry of samples from four sections of the early Cambrian age from the Zhijin region were studied to attain the redox condition and origin of REY. Data from in situ analysis show that REY are mainly contained in francolite, and the two types of francolite (bioclastic and granular) have no distinct difference in REY content (ΣREY). A Ce anomaly indicates an oxic condition in primary seawater. An Eu anomaly and ratios of redox sensitive elements (RSEs) indicate a fluctuating redox condition during phosphorite deposition. Shale-normalized REY patterns of whole rock and francolite show a hat-shaped pattern, indicating the effect of diagenetic processes. The Y/Ho ratio of the selected sections ranges from 38.13 to 61.93, and together with the Y anomaly, La_N/Nd_N ratio, La_N/Sm_N ratio, and La_N/Yb_N ratio, this indicates a seawater origin. This is supported by the Ce/Ce* of the phosphorite that ranges from 0.32 to 0.52 and the Eu/Eu* that ranges from 0.88 to 1.82, which is similar to the characteristics of seawater and deep-sea mud. We also propose a minor contribution of terrigenous debris and influence of diagenesis and hydrothermal processes.

Keywords: rare earth elements and yttrium; phosphorites; francolite; Gezhongwu formation; origin

1. Introduction

Rare earth elements and yttrium (REY) are an extremely important resource in the 21st century. They are widely used in a variety of industries including aerospace, national defense, electronics, petroleum, the chemical industry, metallurgy, textile, ceramics and permanent magnets. Bayan Obo, Mountain Pass, Mount Weld, and South China ion adsorption clay-type are some major REY deposits in the world, among which the Bayan Obo deposit and China's ion adsorption clay-type deposits provide more than 95% of the world's REY production [1,2]. In recent years, with the increase in high-tech industries, the demand for REY in the global market is increasing. Therefore, with the growing need for REY resources, REY in phosphate deposits is considered as a potential REY source to meet the global REY demand [1,3].

REY-enriched phosphate deposits are mainly distributed in Russia, the United States, Vietnam, Egypt, and China [4]. Researchers in the United States have reported that some phosphorites are rich in REY, especially heavy rare earth elements (HREE). The content

of REY (ΣREY) in these phosphorites is higher than that of South China ion adsorption type, with the ΣREY of phosphorites sometimes even reaching 18,000 ppm. The REE-bearing phosphate rocks in Egypt also contain elevated REY with an average content of ~800 ppm, reaching up to 2000 ppm, and show an obvious enrichment of light rare earth element (LREE) relative to the HREE [5,6]. Recently, researchers studied modern marine phosphorites and found a high ΣREY content in seamount phosphorites, with an average of 727 ppm, and a maximum content of 1992 ppm, with high HREE concentrations [3]. In recent years, deep-sea muds have also been proposed as a potential REY resource, which are widely distributed in the Pacific Ocean, Indian Ocean, and Atlantic Ocean [7,8], which contain quite a large amount of REY, reaching up to ~7000 ppm [9].

In China, phosphate deposits are widespread in Yunnan, Guizhou, Sichuan, Hunan, and Hubei Provinces, and the amount of associated rare earth resources is huge, reaching millions of tons [10]. Despite the widespread distribution of phosphate rocks, the distribution of REY-enriched phosphorites is limited. Most reported REY-enriched phosphorites are in the Zhijin region, west Guizhou Province, southwest China, containing 3.5 Mt of REY oxide (REY$_2$O$_3$) resources [11].

Previous studies focused on the Zhijin phosphorites, addressed the identification of minerals in phosphorites [12–14], REY occurrence in francolite [14–19], the depositional environment of the phosphorites [20–22] and the origin of the REY [18,19,23,24]. Francolite is the chief mineral in phosphorite. Other minerals include dolomite, calcite, quartz, chalcedony, clay minerals, pyrite, and limonite [12,13]. It has been agreed that REY are mainly contained in francolite [18,24]. Phase analysis, energy dispersive analysis of X-ray, electron probe micro analyzer (EPMA), and scanning electron microscope showed that the form of REY in francolite is mainly isomorphic substitution, in which REY predominantly substitute for Ca^{2+} [14–19]. The depositional environment of Zhijin phosphorite has been much debated in previous research. Studies investigating the depositional environment of Zhijin phosphorite using Mo isotope analyses indicated that the phosphorite deposit formed in the suboxic-anoxic water [20,21]. However, recent analyses of Mo isotope regarding redox conditions around the Precambrian-Cambrian boundary indicated an oxic condition prevailed in Central Guizhou during the early Cambrian [25]. However, Fe isotope analyses suggest fluctuating oxic–suboxic seawater conditions at the same time [26,27].

The origin of REY in the Zhijin phosphorite has been discussed for a long time, but no clear conclusions have been drawn. Seawater is an important source of REY. In phosphate grains, REY can be incorporated from seawater mainly during the transportation and redeposition phase when the grains are in direct contact with seawater [28]. In the Zhijin deposit, the seawater origin of REY is supported by Sr-Nd isotope data [29], the relationship between the mineral/seawater REY partition coefficients and the logarithm of the ionic radius [19]. Moreover, the mixing of normal seawater and hydrothermal fluids has also been considered as one of the possible REY origins of the Zhijin phosphorite based on the following geochemistry characteristics [18,23,24]: (1) the mixed REY pattern of normal seawater and hydrothermal fluids; (2) Fe/Ti > 20, (Fe + Mn)/Ti > 25 and Al/(Al + Fe + Mn) < 0.35; (3) U/Th > 1; and (4) the enrichment of As and Sb. The hydrothermal influence has been shown by the observation of hydrothermal veins, hydrothermal minerals (e.g., anatase and fluorite) and hydrothermally transformed minerals (e.g., fluorapatite and zircon) [30]. Terrigenous materials along with organic matter are also considered the principal source of REY in phosphatic rocks [31]. However, there is no reported evidence of a terrigenous origin in Zhijin phosphorite.

Here, we present the major and trace elements of four representative sections from the Zhijin region to comprehensively discuss the REY distribution in Zhijin phosphorites. To better discuss the distribution of REY in single mineral, we analyze the in situ REY concentrations in francolite and dolomite from the Linfeichang (LFC) section. Moreover, we discuss some diagnostic parameters and ratios to define the REY origin as well as diagenetic processes. Based on our results, we propose that seawater is the main origin of REY, and terrigenous materials have little influence.

2. Geology Setting

The Zhijin region is located in the Yangtze Platform, southern China, which contains a succession of Ediacaran to Early Cambrian age stratigraphy with different paleoenvironmental settings, including a platform, transition belt, and basin belt [26,32] (Figure 1). The Yangtze paleogeographic block was the site of massive phosphogenesis between 580 and 520 Ma (Neoproterozoic III–Cambrian) [33], resulting in two significant phosphorite forming periods: Ediacaran and Early Cambrian, corresponding to phosphate deposits in the Doushantuo Formation and Gezhongwu Formation, respectively, in Guizhou Province. The Zhijin phosphorite deposit is located within the carbonate platform inside the Yangtze Block (Figure 1), preserving shallow-water sediments [22].
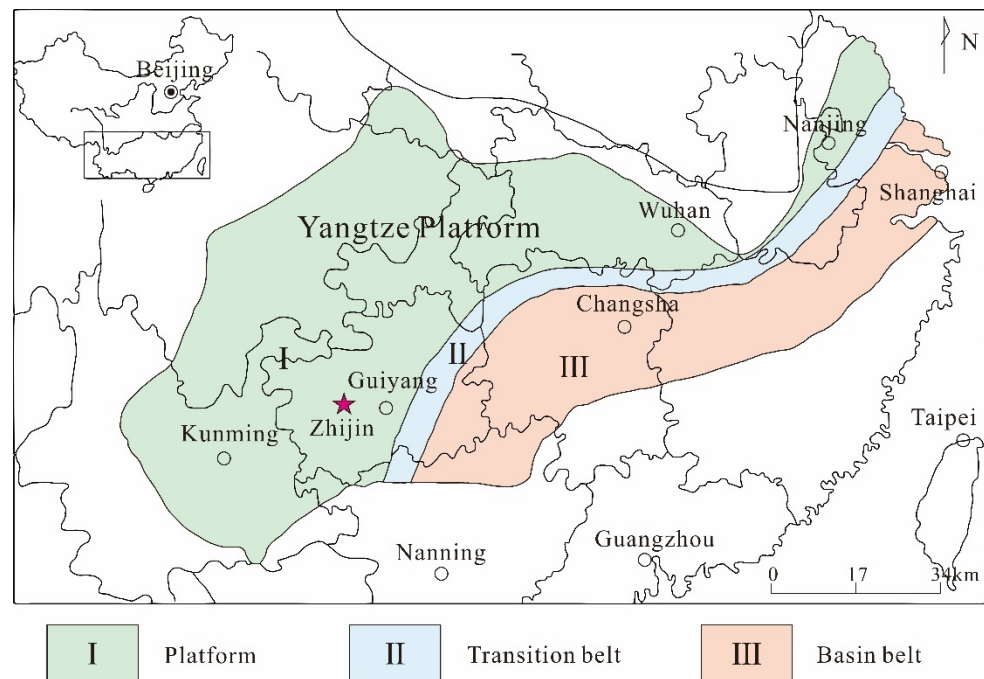

Figure 1. Simplified paleogeographic map of the Yangtze Platform during the early Cambrian, modified from Steiner et al. (2001) [34] and Guo et al. (2007) [32]. The star represents the studied region.

Xinhua and Lijiazhai phosphate ore blocks are two typical ore blocks in the Zhijin deposit. The LFC section, the Gaoshan (GS) section, and the ZKX002 section belong to the Xinhua phosphate ore block, and the Lijiazhai (LJZ) section belongs to the Lijiazhai phosphate ore block (Figure 2a). The Lijiazhai ore block is 17 km to the southeast of the Xinhua ore block (Figure 2a). In the Zhijin region, the phosphate rocks of the early Cambrian Gezhongwu Formation conformably overlay the dolomite of the Dengying Formation and are in turn, conformably overlain by the siltstone of the Niutitang Formation and equivalent strata (Figure 2b).

The LFC section is a typical section of the Gezhongwu Formation. It is composed of a lower layer and an upper layer (Figure 2b). The lower layer is mainly interbedded with dolomitic phosphorite and phosphatic dolomite, while the upper layer is mainly interbedded with siliceous dolomitic phosphorite and siliceous phosphatic dolomite. The lower layer mainly consists of bioclastic phosphorites, while the upper layer mainly contains granular phosphorite with less bioclastic components. The structure of the ore body is banded and massive. The banded phosphorite is interbedded by dark gray phosphorite and light gray phosphatic dolomite. The thickness of dolomitic phosphorite is 2–5 cm, and that of phosphatic dolomite is about 10–30 cm.
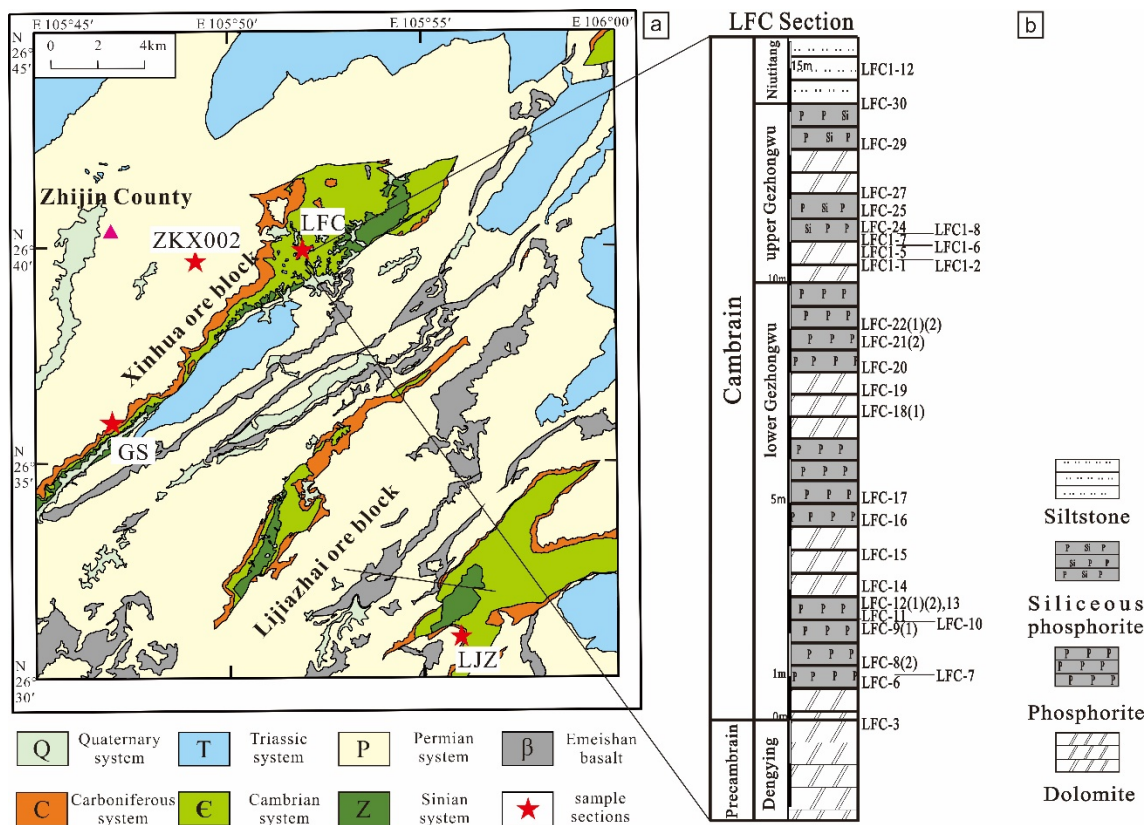
Figure 2. (**a**) Geological map of the Zhijin region. The pink triangle represents Zhijin County, and the red stars are the sampling locations (LFC is the Linfeichang section; Gs is the Gaoshan section; LJZ is the Lijiazhai section.). (**b**) Stratigraphic columns and sampling sites of the LFC Section.

The Gaoshan (GS) section is located in the southeast of Zhijin County and contains a relatively high content of P and REY. The thickness of the Gezhongwu Formation in this section is about 14 m, and it is mainly composed of light to dark gray phosphorite. The Lijiazhai (LJZ) section contains a relatively low content of P and REY. The thickness of Gezhongwu Formation in this section is about 9 m, and it is mainly composed of light gray phosphatic dolomite. The ZKX002 section belongs to the lower layer of the Zhijin deposit, and samples were obtained from drill core. The thickness of Gezhongwu Formation in this section is about 14 m, and it is mainly composed of black to gray compact massive phosphorite and light gray phosphatic dolomite.

3. Materials and Methods

3.1. Samples

Phosphorite samples of the Gezhongwu Formation were collected from the following four sections (Figure 2a; marked by red stars): the LFC section (N = 30), the GS section (N = 4), the LJZ section (N = 5), and the ZKX002 section (N = 6). The sampling sites are shown in Figure 2b, with the LFC section given as an example, because the samples are well-exposed, fresh, and sequential.

3.2. Methods

The micro-textures of minerals were observed using a JSM-7800F field emission SEM at the State Key Laboratory of Deposit Geochemistry, Institute of Geochemistry, Chinese Academy of Sciences. The backscattered electron image (BSE) was collected with a 20 Kv, 4.5 mA beam current.

Samples used for geochemical analyses were cut with a cutting machine to remove stale surfaces and visible veins. Then, the samples were ground to 200-mesh powders, and

the subsequent major and trace element analyses were conducted on these powders. The major elements of the whole rock were analyzed by ALS Minerals (Guangzhou, China) Co., Ltd., and this analysis of phosphate rock was carried out using the X-ray fluorescence spectrometry melting method (ME-XRF24 and ME-XRF26s). Trace elements of whole rocks were measured using a quadrupole inductively coupled plasma mass spectrometer (Q-ICP-MS) at the State Key Laboratory of Deposit Geochemistry, Institute of Geochemistry, Chinese Academy of Sciences, with a relative standard deviation that was generally better than 10%. Fifty milligrams of the powdered samples were completely digested using a mixture of HF and HNO_3 solution. The internal standard was a 40 ng/mL Rh solution. The standard materials for samples (ΣREY > 500 ppm) from the GS, LJZ and ZKX002 sections were OU-6, AGV-2, and GBPG-1. The standard materials for the other samples were AGV-2, AMH-1, and GBPG-1. The detection limits were as follows: Tb, Ho, Lu, and Tm (0.01 ppm); Er, Eu, Sm, Pr, and Yb (0.03 ppm); Ce, Gd, and Dy (0.05 ppm); Nd (0.1 ppm); Y and La (0.5 ppm).

In situ analysis of francolite and dolomites was carried out at the State Key Laboratory of Deposit Geochemistry, Institute of Geochemistry, Chinese Academy of Sciences. The laser ablation system utilized a 193 nm excimer laser system produced by Coherent, and the ICP-MS used an Agilent 7900 inductively coupled plasma mass spectrometer. Each acquisition cycle included a 20 s blank signal and a 50 s sample signal. Ablation was carried out with a 44 μm beam. SRM610 and SRM612 were used as external standards. Durango was used as the apatite calibration standard and MACS as the carbonate calibration standard. The multiple external standard-single internal standard method [35] was used for the quantitative calculation of element content, and Ca obtained by electron probe was used as the internal standard.

4. Results

4.1. Francolite Micro-Textures

Phosphate minerals, typically identified as apatite or francolite, occur as fine-grained aggregates. Francolite is the major REY-bearing mineral in the phosphorites, and it is cemented mainly by dolomite (Figure 3a–c), with lesser calcite, pyrite, quartz, and clay minerals. In the GS section, quartz is a more common component of the cement than in the other localities. Based on the shape of minerals, francolite in Zhijin phosphorite are divided into granular (Figure 3a,d–f) and bioclastic (Figure 3b,c,f) sub-types. The granular (Figure 4a–d) and bioclastic (Figure 4e–l) francolite can be observed better on BSE images. The bioclastic francolite includes a large number of *Zhijinitids* [36] (Figures 3c and 4h,k,l), a particular kind of small shelly fossil found in the Zhijin region.

In the LFC section, bioclastic francolite and granular francolite are heterogeneously distributed through the section, in which the bioclastic francolite grains are more heavily distributed in the lower layer than in the upper layer. The length of columnar francolite is 50–200 μm, and the width is 20–50 μm, and the diameter of granular francolite is approximately 50 μm. The francolite grains are predominantly oriented in the samples with high REY level, and the bioclastic francolite grains are closely packed (Figure 3b). Otherwise, in the ZKX002 section, the distribution of two types of francolites is relatively uniform. The size of the francolite is similar to that in the LFC section. In the GS section and the LJZ section, the majority of francolite is granular.
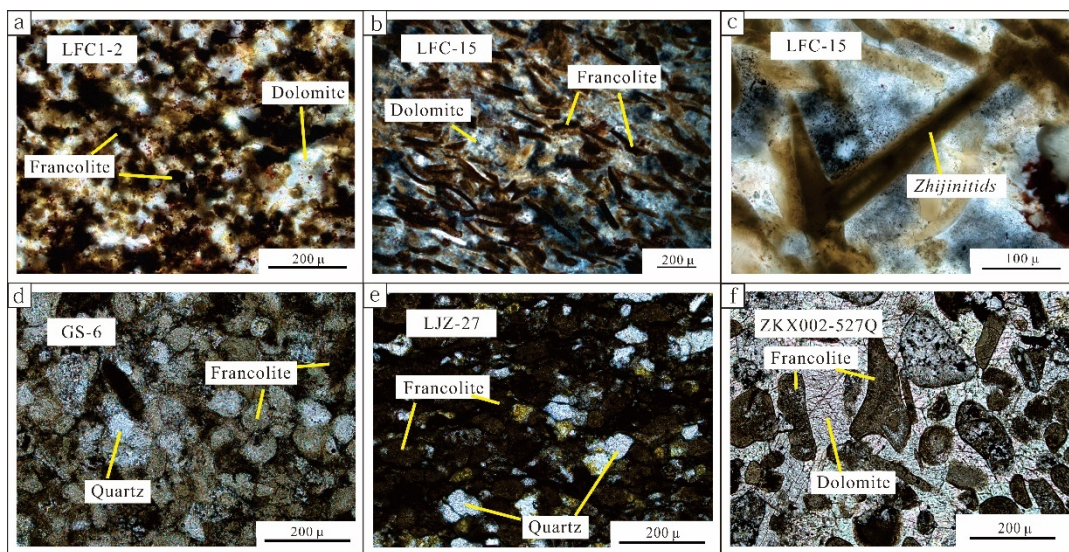
Figure 3. Microstructure of phosphorites in the Zhijin region (under transmitted light, plane polarized). (**a**) Granular francolite from the LFC section; (**b**) bioclastic francolite from the LFC section; (**c**) *Zhijinitids* from the LFC section; (**d**) granular francolite from the GS section; (**e**) granular francolite from the LJZ section; (**f**) bioclastic and granular francolite from the ZKX002 section.
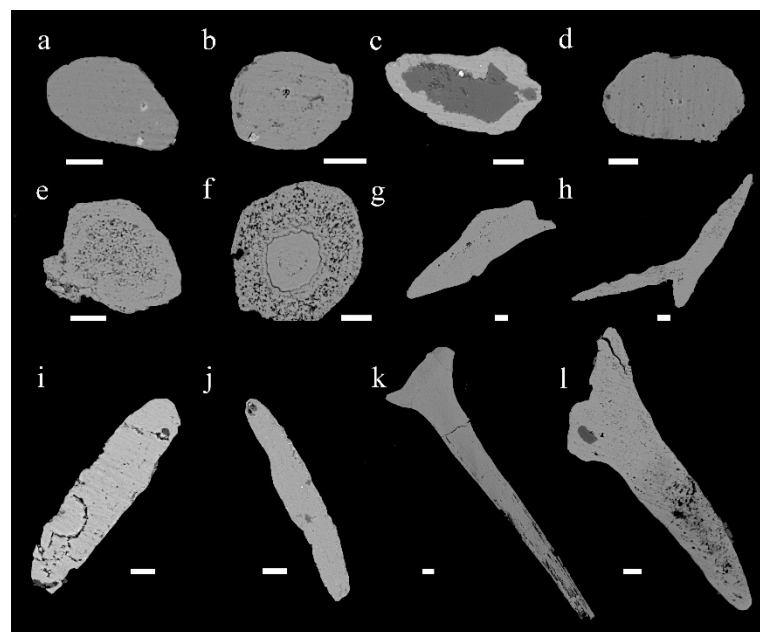
Figure 4. Different back-scattered electron images (BSE) of francolite in the Zhijin phosphorites. Each scale bar shown inset represents 20 μm. (**a**–**d**) Granular francolite; (**e**–**l**) bioclastic francolite; (**e**,**f**) the cross section of the bioclastic francolite.

4.2. Bulk Major and Trace Elements

The major element contents of the Zhijin phosphorites are shown in Table 1. In all of the samples from the Zhijin phosphorites, the P_2O_5 content ranges from 1.86% to 38.50%, with an average of 18.39%; the F content ranges from 0.30% to 4.10%, with an average of 1.86%; the CaO content varies from 13.25% to 53.80%, with an average of 36.18%. In the four selected sections, the average contents of P_2O_5 are as follows: the GS section (P_2O_5 = 32.37%) > the lower layer of the LFC section (P_2O_5 = 20.13%) > the upper layer of the LFC section (P_2O_5 = 18.61%) > the ZKX002 section (P_2O_5 = 15.63%) > the LJZ section (P_2O_5 = 6.2%). The GS section is the section with the highest P_2O_5 content. In contrast, the

LJZ section has the lowest P_2O_5 content. In the LFC section, the P_2O_5 content of samples from the upper layer is lower than that of the lower layer.

The ΣREY of the Zhijin phosphorites exhibit a relatively large range of 95.71–1936.69 ppm (Table 2), with an average value of 943.30 ppm. The average contents of ΣREY of the four sections are as follow: the GS section (ΣREY = 1591.48 ppm) > the upper layer of the LFC section (ΣREY = 1072.93 ppm) > the lower layer of the LFC section (ΣREY = 892.83 ppm) > the ZKX002 section (ΣREY = 804.88 ppm) > the LJZ section (ΣREY = 497.49 ppm). The ΣREY of the dolomites and the siltstones are low, with an average of 16.30 and 175.03 ppm, respectively. The Ce/Ce* ranges from 0.34 to 0.52, with an average of 0.40, showing significantly negative anomalies (Table 2). Additionally, the Eu/Eu* ranges from 0.90 to 1.62, with an average of 1.16, showing slightly negative or positive anomalies (Table 2). The LREE (La − Eu)/HREE (Gd − Lu + Y) ratio is over 1, with an average value of 1.39, showing that LREE is more enriched than HREE.

The major element correlations of ΣREY (Figure 5) show that ΣREY has a significantly positive correlation with P_2O_5, CaO, and F, but a negative correlation with MgO. In addition, ΣREY has no obvious correlation with SiO_2 and Fe_2O_3.

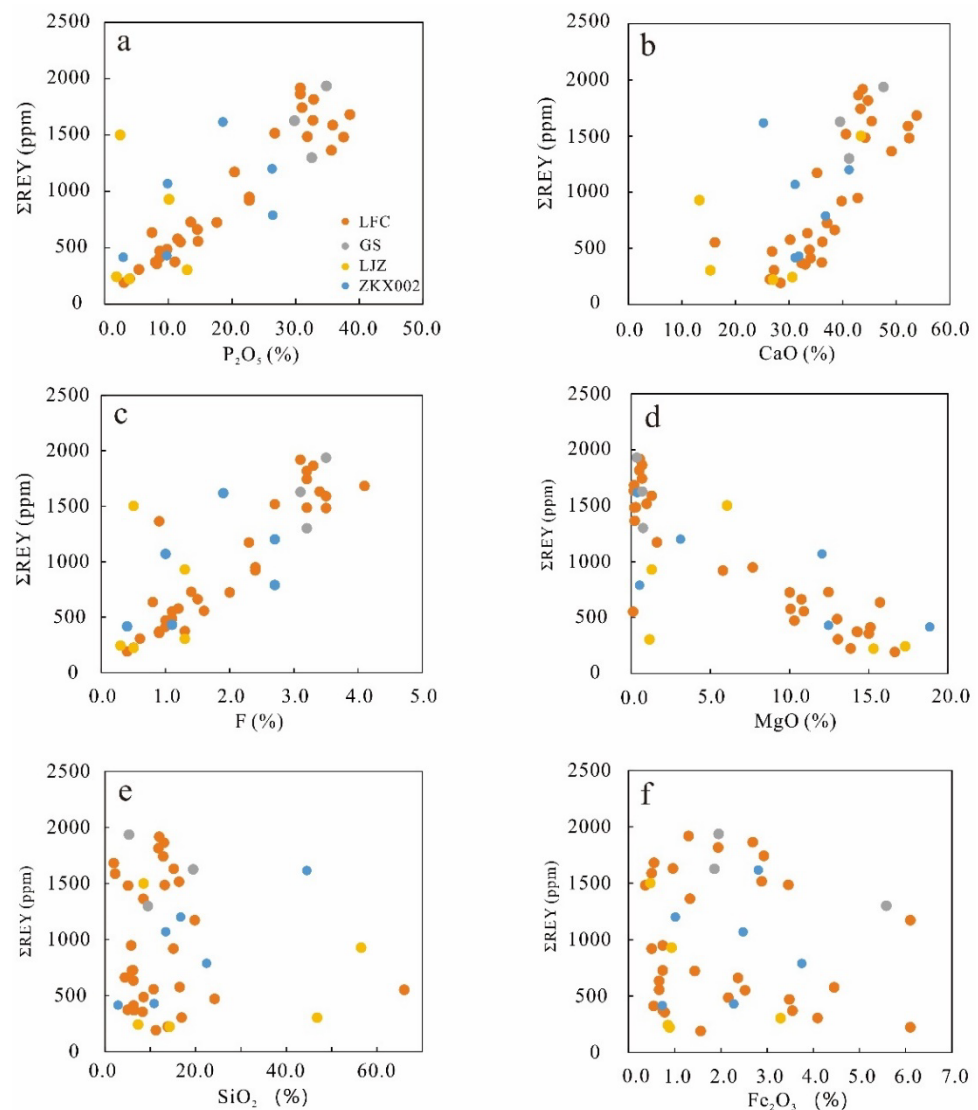**Figure 5.** The correlations between ΣREY and some major elements in phosphorite from the Zhijin region. (**a**) ΣREY vs. P_2O_5. (**b**) ΣREY vs. CaO. (**c**) ΣREY vs. F. (**d**) ΣREY vs. MgO. (**e**) ΣREY vs. SiO_2. (**f**) ΣREY vs. Fe_2O_3.

Table 1. Some selected major elements of Zhijin phosphorites (wt.%).

Stratum	Sample		P_2O_5	CaO	F	MgO	SiO_2	Al_2O_3	TFe_2O_3	MnO	K_2O	Na_2O	LOI
Upper Gezhongwu	LFC1-8	Phosphorite	30.70	43.70	3.10	0.54	11.96	2.49	1.30	0.01	0.80	0.06	5.45
	LFC1-7	Phosphatic dolomite	5.36	27.20	0.60	13.05	16.92	0.83	4.09	0.46	0.29	0.03	30.62
	LFC1-6	Phosphorite	26.70	40.60	2.70	0.97	16.35	2.02	2.88	0.06	0.68	0.04	7.03
	LFC1-5	Phosphatic dolomite	3.91	26.40	0.50	13.85	13.83	0.96	6.10	0.32	0.31	0.01	32.76
	LFC1-2	Phosphorite	20.40	35.20	2.30	1.62	19.81	2.50	6.10	0.14	0.81	0.05	10.82
	LFC1-1	Phosphatic dolomite	8.64	26.80	1.00	10.30	24.19	0.93	3.48	0.27	0.33	0.03	23.99
	LFC-30	Phosphorite	32.80	44.70	3.20	0.51	11.80	2.72	1.94	0.02	0.81	0.07	2.63
	LFC-29	Phosphatic dolomite	3.01	28.40	0.40	16.65	11.22	0.61	1.56	0.24	0.21	0.03	37.60
	LFC-27	Phosphorite	30.70	42.90	3.30	0.68	13.00	3.11	2.69	0.02	1.02	0.08	3.41
	LFC-25	Phosphorite	31.00	43.30	3.20	0.68	12.86	2.07	2.93	0.03	0.75	0.06	3.37
	LFC-24	Phosphatic dolomite	11.45	30.20	1.20	10.05	16.47	1.34	4.45	0.23	0.43	0.04	23.70
Lower Gezhongwu	LFC-22 (2)	Phosphorite	32.70	45.40	3.40	0.17	15.19	0.52	0.96	0.04	0.17	0.05	1.90
	LFC-22 (1)	Phosphatic dolomite	11.90	16.15	1.10	0.11	66.02	0.63	2.52	0.17	0.16	0.03	1.01
	LFC-21 (2)	Phosphorite	31.80	44.20	3.20	0.29	13.18	1.07	3.46	0.27	0.36	0.05	2.54
	LFC-20	Phosphatic dolomite	9.79	33.80	1.10	13.00	8.52	0.31	2.16	0.28	0.12	0.03	31.15
	LFC-19	Phosphatic dolomite	14.55	38.50	1.50	10.75	4.42	0.49	2.37	0.40	0.18	0.05	27.25
	LFC-18 (1)	Phosphorite	35.60	49.10	0.90	0.22	8.47	0.55	1.33	0.13	0.21	0.07	2.61
	LFC-17	Phosphatic dolomite	7.95	32.30	0.90	14.30	6.39	0.36	3.55	0.33	0.13	0.03	33.69
	LFC-16	Phosphorite	22.70	42.80	2.40	7.67	5.80	0.39	0.74	0.07	0.15	0.07	18.06
	LFC-15	Phosphatic dolomite	17.60	37.10	2.00	10.00	5.92	0.73	1.43	0.11	0.25	0.05	23.25
	LFC-14	Phosphatic dolomite	13.50	37.10	1.40	12.45	6.17	0.26	0.74	0.09	0.10	0.05	28.44
	LFC-13	Phosphatic dolomite	7.41	33.40	0.80	15.70	6.26	0.28	0.66	0.10	0.11	0.03	35.50
	LFC-12 (2)	Phosphatic dolomite	11.00	36.10	1.30	14.25	4.99	0.28	0.74	0.09	0.11	0.05	32.01
	LFC-12 (1)	Phosphorite	35.80	52.20	3.50	1.29	2.26	0.22	0.50	0.02	0.10	0.11	4.71
	LFC-11	Phosphorite	22.70	39.80	2.40	5.79	15.09	0.58	0.50	0.05	0.21	0.06	13.78
	LFC-10	Phosphatic dolomite	8.63	34.00	1.00	15.10	6.31	0.32	0.54	0.10	0.12	0.03	34.16
	LFC-9 (1)	Phosphorite	37.50	52.40	3.50	0.19	5.08	0.38	0.36	0.02	0.14	0.05	2.19
	LFC-8 (2)	Phosphatic dolomite	14.65	36.20	1.60	10.90	10.74	0.55	0.66	0.07	0.20	0.05	25.00
	LFC-7	Phosphorite	38.50	53.80	4.10	0.18	1.94	0.38	0.55	0.02	0.15	0.11	2.24
	LFC-6	Phosphatic dolomite	8.17	33.00	0.90	15.00	8.29	0.54	0.78	0.10	0.18	0.04	33.53
Upper Gezhongwu	GS-13	Phosphorite	32.50	41.20	3.20	0.75	9.47	3.13	5.58	0.02	1.04	0.14	7.43
	GS-10	Phosphorite	34.80	47.60	3.50	0.38	5.32	2.53	1.95	0.02	0.70	0.14	3.06
	GS-6	Phosphorite	29.80	39.50	3.10	0.70	19.45	2.85	1.86	0.01	0.98	0.13	3.07
Lower Gezhongwu	LJZ-5	Phosphatic dolomite	2.44	43.40	0.50	6.05	8.52	0.74	0.47	0.05	0.28	<0.01	29.90
	LJZ-12	Phosphatic dolomite	1.86	30.60	0.30	17.30	7.32	0.43	0.85	0.14	0.17	<0.01	41.08
	LJZ-17	Phosphatic dolomite	3.84	27.00	0.50	15.30	14.25	1.66	0.89	0.08	0.72	<0.01	34.80
	LJZ-23	Phosphatic dolomite	12.95	15.30	1.30	1.15	46.80	9.36	3.29	<0.01	4.35	0.09	4.46
	LJZ-27	Phosphatic dolomite	10.10	13.25	1.30	1.29	56.50	9.38	0.93	<0.01	4.52	0.10	3.09

Table 1. *Cont.*

Stratum	Sample		P$_2$O$_5$	CaO	F	MgO	SiO$_2$	Al$_2$O$_3$	TFe$_2$O$_3$	MnO	K$_2$O	Na$_2$O	LOI
	ZKX002-520.5	Phosphorite	26.40	36.80	2.70	0.52	22.40	2.25	3.75	0.03	0.74	0.11	3.88
	ZKX002-523	Phosphorite	18.55	25.20	1.90	0.38	44.50	1.86	2.81	0.04	0.58	0.08	3.82
Lower Gezhongwu	ZKX002-527S	Phosphorite	26.30	41.20	2.70	3.11	16.70	0.47	1.01	0.09	0.15	0.12	8.25
	ZKX002-527Q	Phosphatic dolomite	9.87	31.10	1.00	12.05	13.40	0.32	2.48	0.32	0.10	0.03	27.28
	ZKX002-528.5	Phosphatic dolomite	9.76	31.80	1.10	12.45	10.85	0.99	2.28	0.34	0.28	0.02	28.31
	ZKX002-531Q	Phosphatic dolomite	2.91	31.10	0.40	18.85	2.91	0.38	0.73	0.15	0.12	<0.01	41.74

LOI is an abbreviation for loss on ignition. LFC represents the Linfeichang section; GS represents the Gaoshan section; LJZ represents the Lijiazhai section.

Table 2. The REY content (ΣREY, ppm) of the Zhijin phosphorites and phosphatic dolomites (bulk-rock analyses).

Stratum	Sample		La	Ce	Pr	Nd	Sm	Eu	Gd	Tb	Dy	Y	Ho	Er	Tm	Yb	Lu	ΣREY
	LFC1-8	Phosphorite	351.00	293.00	69.70	335.00	62.60	23.12	71.09	9.90	58.20	582.00	12.20	30.30	3.37	14.90	1.87	1918.24
	LFC1-7	Phosphatic dolomite	57.50	45.80	10.60	50.20	9.13	3.30	10.17	1.54	8.63	98.80	1.81	4.76	0.52	2.74	0.33	305.84
	LFC1-6	Phosphorite	270.00	238.00	55.40	267.00	51.50	18.12	54.64	7.92	44.60	461.00	9.21	23.50	2.52	12.00	1.51	1516.93
	LFC1-5	Phosphatic dolomite	40.20	35.30	7.69	37.20	7.14	2.41	7.62	1.15	6.44	71.30	1.34	3.43	0.40	2.11	0.27	224.00
	LFC1-2	Phosphorite	204.00	178.00	43.20	210.00	41.00	14.57	43.58	5.94	35.20	360.00	7.03	17.90	1.99	9.33	1.20	1172.94
Upper Gezhongwu	LFC1-1	Phosphatic dolomite	89.50	71.60	16.60	78.70	14.30	4.69	16.06	2.26	13.30	149.00	2.81	7.44	0.78	4.05	0.51	471.60
	LFC-30	Phosphorite	367.00	245.00	59.40	275.00	48.60	10.86	56.82	8.13	53.60	623.00	11.90	32.30	3.80	18.70	2.52	1816.63
	LFC-29	Phosphatic dolomite	39.10	26.80	6.00	28.20	4.78	1.15	5.76	0.88	5.42	65.50	1.20	3.41	0.43	2.53	0.33	191.48
	LFC-27	Phosphorite	378.00	264.00	63.60	302.00	50.80	11.73	60.54	8.83	54.80	606.00	11.80	31.20	3.36	15.70	1.95	1864.31
	LFC-25	Phosphorite	357.00	244.00	58.80	277.00	47.30	11.04	54.60	8.11	52.40	573.00	10.90	28.50	3.12	15.30	1.80	1742.87
	LFC-24	Phosphatic dolomite	123.00	82.30	18.50	85.20	14.30	3.57	16.83	2.56	16.00	195.00	3.49	9.41	1.10	5.42	0.68	577.36
	LFC-22 (2)	Phosphorite	328.00	230.00	59.30	293.00	51.80	14.82	56.11	8.21	48.40	490.00	9.77	25.10	2.77	13.10	1.64	1632.02
	LFC-22 (1)	Phosphatic dolomite	110.00	78.60	20.70	95.60	17.80	5.48	19.75	2.81	16.60	167.00	3.32	8.38	0.93	4.46	0.60	552.03
	LFC-21 (2)	Phosphorite	300.00	205.00	55.70	263.00	46.00	12.61	50.33	7.32	43.90	453.00	9.10	23.40	2.55	12.70	1.50	1486.11
	LFC-20	Phosphatic dolomite	102.00	66.00	17.60	81.10	14.10	3.05	15.17	2.31	13.50	156.00	2.92	7.68	0.86	4.32	0.53	487.14
	LFC-19	Phosphatic dolomite	142.00	90.70	23.70	109.00	18.60	4.15	20.26	3.05	18.60	210.00	3.92	10.40	1.17	6.05	0.73	662.32
	LFC-18 (1)	Phosphorite	277.00	203.00	51.30	236.00	43.50	15.21	52.18	6.62	37.30	402.00	7.29	19.20	2.06	10.40	1.21	1364.27
	LFC-17	Phosphatic dolomite	75.10	53.70	13.30	60.30	12.10	4.32	14.19	1.84	10.10	114.00	2.03	5.46	0.56	3.08	0.37	370.44
Lower Gezhongwu	LFC-16	Phosphorite	196.00	131.00	34.20	159.00	29.20	10.03	35.52	4.52	25.30	294.00	5.46	13.80	1.60	7.95	0.94	948.52
	LFC-15	Phosphatic dolomite	151.00	102.00	26.20	118.00	22.10	7.82	26.61	3.39	18.70	225.00	3.96	10.80	1.21	6.22	0.71	723.71
	LFC-14	Phosphatic dolomite	149.00	104.00	26.20	120.00	22.00	7.85	26.76	3.45	19.90	225.00	4.03	10.80	1.21	6.34	0.73	727.27
	LFC-13	Phosphatic dolomite	130.00	91.30	23.20	106.00	20.40	6.61	23.64	3.05	16.90	194.00	3.41	9.45	1.02	5.35	0.64	634.97
	LFC-12 (2)	Phosphatic dolomite	81.50	48.50	12.80	56.10	9.80	2.46	11.64	1.68	9.70	127.00	2.13	5.84	0.73	3.98	0.46	374.31
	LFC-12 (1)	Phosphorite	352.00	208.00	58.40	260.00	45.70	10.55	53.82	7.13	42.80	501.00	9.13	23.20	2.59	13.10	1.51	1588.93
	LFC-11	Phosphorite	203.00	122.00	34.10	149.00	27.00	6.33	32.20	4.28	25.20	287.00	5.24	14.50	1.44	8.12	0.89	920.30
	LFC-10	Phosphatic dolomite	89.40	52.60	14.50	62.20	11.10	2.70	13.51	1.81	10.80	140.00	2.37	6.38	0.77	4.16	0.50	412.79

Table 2. *Cont.*

Stratum	Sample		La	Ce	Pr	Nd	Sm	Eu	Gd	Tb	Dy	Y	Ho	Er	Tm	Yb	Lu	ΣREY
	LFC-9 (1)	Phosphorite	328.00	192.00	54.10	235.00	41.30	9.83	49.58	6.88	39.00	481.00	8.30	21.50	2.41	12.00	1.38	1482.28
	LFC-8 (2)	Phosphatic dolomite	122.00	73.60	19.40	87.60	15.00	3.85	18.99	2.49	15.00	181.00	3.19	8.42	1.02	4.95	0.63	557.13
	LFC-7	Phosphorite	351.00	229.00	61.70	275.00	48.90	11.78	57.87	8.02	46.40	539.00	9.76	25.90	2.73	14.20	1.59	1682.85
	LFC-6	Phosphatic dolomite	75.90	46.40	12.10	53.70	9.44	2.37	11.21	1.57	9.31	122.00	1.97	5.62	0.67	3.63	0.43	356.32
Upper Gezhongwu	GS-13	Phosphorite	271.00	177.00	42.30	197.00	36.40	7.87	42.10	6.01	39.30	433.00	8.54	22.00	2.64	13.10	1.66	1299.92
	GS-10	Phosphorite	388.00	268.00	64.30	288.00	54.20	11.50	53.80	7.86	52.80	686.00	11.70	29.30	3.36	15.90	1.97	1936.69
	GS-6	Phosphorite	340.00	258.00	54.80	261.00	51.10	10.70	55.90	7.87	49.00	484.00	10.30	25.60	2.99	14.50	1.84	1627.60
	GS-3	Phosphorite	318.00	216.00	48.40	232.00	44.00	9.10	49.90	7.00	45.20	478.00	9.67	24.60	3.00	14.90	1.92	1501.69
Lower Gezhongwu	LJZ-5	Phosphatic dolomite	50.20	43.40	8.98	36.60	6.14	1.24	6.40	1.35	7.29	70.80	1.76	4.69	0.63	3.04	0.47	242.99
	LJZ-12	Phosphatic dolomite	47.70	37.40	8.47	34.30	5.52	1.36	5.92	1.25	6.72	64.80	1.64	3.88	0.58	2.56	0.41	222.51
	LJZ-17	Phosphatic dolomite	61.50	51.30	11.10	48.30	8.11	1.80	8.69	1.74	9.59	88.70	2.27	5.71	0.83	3.67	0.53	303.85
	LJZ-23	Phosphatic dolomite	188	145	34.8	156	29.7	6.25	32.6	4.59	28.8	271	6.06	15.1	1.76	8.73	1.1	929.49
	LJZ-27	Phosphatic dolomite	157	129	30.4	132	25.5	5.05	27	3.91	25.1	225	5.24	13.1	1.53	7.8	1	788.63
Lower Gezhongwu	ZKX002-520.5	Phosphorite	308.00	239.00	58.8	270.00	57.9	12.5	63.3	8.96	56	482.00	11.4	28.1	3.22	15.4	1.93	1616.51
	ZKX002-523	Phosphorite	253.00	173.00	42.2	205.00	38.9	8.08	42.9	5.89	36.6	356.00	7.57	18.6	2.08	9.86	1.21	1200.89
	ZKX002-727S	Phosphorite	226.00	138.00	38.8	174.00	32.3	6.8	35.6	5.06	32.5	343.00	6.89	17.4	2.07	10	1.25	1069.67
	ZKX002-527Q	Phosphatic dolomite	86.90	67.20	18.10	71.80	13.60	2.96	15.35	2.46	13.10	122.00	3.20	7.92	0.91	4.57	0.60	430.66
	ZKX002-528.5	Phosphatic dolomite	84.00	63.40	17.40	69.00	13.10	3.42	14.55	2.35	12.40	119.00	3.10	7.88	0.93	4.76	0.58	415.86
	ZKX002-531S	Phosphatic dolomite	18.50	17.60	3.25	13.60	2.60	0.80	2.98	0.47	2.62	29.70	0.65	1.56	0.21	1.03	0.13	95.71

Anomalous abundances of Ce, suggested by Ce/Ce* ratios, are calculated by $Ce_N/(La_N \times Pr_N)^{1/2}$.

4.3. In Situ REY of Francolite and Dolomite

Forty francolite and ten dolomite minerals from four samples from the LFC section were selected for in situ analysis of their REY composition. Both bioclastic and granular francolite were studied, and the ΣREY (ppm) and elemental ratios are given in Table 3 and Table S2. Some selected major element contents are given in Table S3. The ΣREY of francolite from the lower layer ranges from 1640 to 2054 ppm, with an average of 1836 ppm. In contrast, the ΣREY of francolite from the upper layer ranges from 2054 to 2600 ppm, with an average of 2294 ppm. The upper layer of the LFC section contains a relatively high ΣREY, which is consistent with the result of the whole rock trace element chemistry. As for different types of francolite, the ΣREY of bioclastic francolite ranges from 1664 to 2054 ppm, with an average of 1825 ppm, and the ΣREY of granular francolite ranges from 1640 to 2600 ppm, with an average of 2168 ppm; seemingly, the granular francolite is more enriched in ΣREY than the bioclastic francolite. However, if we focus on the two types of francolite, both from the lower layer, the average ΣREY of both types is similar. In other words, there is no obvious ΣREY difference between granular francolite and bioclastic francolite from given stratum, but the upper layer has higher ΣREY than the lower layer. The ΣREY of dolomite ranges from 44 to 95 ppm, which is much lower than that of francolite.

Table 3. In situ ΣREY of the francolite and dolomite from the LFC section (ppm).

Sample (Type)	Spot	La	Ce	Pr	Nd	Sm	Eu	Gd	Tb	Dy	Y	Ho	Er	Tm	Yb	Lu	ΣREY
LFC1-2 (granular francolite)	1-2-1-A	409.65	289.25	66.63	316.96	59.82	17.85	72.82	9.39	57.14	687.99	12.38	31.12	3.40	16.40	1.90	2052.71
	1-2-1-B	454.62	339.90	77.36	365.66	69.65	23.64	84.02	10.51	62.48	730.63	13.60	33.85	3.71	17.96	2.23	2289.82
	1-2-1-C	455.48	349.21	80.62	381.03	73.58	26.35	86.76	10.76	64.49	729.65	13.63	33.32	3.64	17.47	2.08	2328.05
	1-2-1-D	499.29	349.48	76.37	350.80	64.06	18.63	77.59	9.87	60.46	740.41	13.29	33.81	3.89	19.04	2.36	2319.34
	1-2-2-A	419.61	376.72	91.17	462.19	96.22	40.29	110.61	13.05	73.28	761.09	14.85	35.11	3.57	16.06	1.80	2515.63
	1-2-2-B	486.67	362.92	81.14	381.91	71.82	22.99	85.69	10.85	65.12	768.14	14.01	35.16	3.90	18.73	2.23	2411.28
	1-2-2-C	449.06	327.23	72.89	336.70	63.09	18.93	76.72	9.68	59.07	707.69	12.76	32.31	3.59	17.52	2.11	2189.36
	1-2-2-D	493.49	365.51	81.02	378.13	71.89	22.98	85.05	10.97	65.34	768.78	14.00	35.18	3.86	18.61	2.29	2417.10
LFC-27 (granular francolite)	27-1-A	545.90	321.73	73.54	327.67	58.78	12.86	73.39	9.86	62.49	758.35	13.60	34.70	3.94	18.89	2.26	2317.94
	27-1-B	549.07	314.76	71.68	321.15	56.82	12.65	71.55	9.61	62.22	754.67	13.59	35.19	3.90	19.59	2.26	2298.71
	27-1-C	550.93	320.23	73.42	328.28	58.15	12.99	73.06	9.85	63.06	774.59	13.95	35.56	3.97	20.06	2.33	2340.42
	27-1-D	537.62	306.30	69.99	308.56	53.74	11.73	68.95	9.18	59.67	741.40	13.08	34.30	3.83	19.18	2.30	2239.83
	27-1-E	493.11	298.05	69.55	317.53	57.27	13.50	73.54	9.82	61.55	738.46	13.47	33.92	3.69	18.20	2.12	2203.78
	27-1-F	465.71	291.85	69.91	321.85	59.51	13.83	74.67	9.98	62.41	735.87	13.44	33.68	3.62	17.27	1.96	2175.58
	27-1-G	494.84	286.07	65.52	299.20	53.26	12.12	69.02	9.23	59.60	742.24	13.13	34.15	3.86	19.39	2.29	2163.92
	27-2-A	517.22	304.56	69.84	314.55	56.29	12.67	71.45	9.49	60.99	742.17	13.39	34.19	3.85	19.19	2.25	2232.10
	27-2-B	563.55	359.06	84.33	385.42	70.10	17.17	88.41	11.77	73.56	863.29	15.92	40.14	4.32	20.82	2.41	2600.27
	27-2-C	483.47	295.31	69.22	318.39	57.29	13.50	73.74	9.94	64.07	761.65	13.78	35.86	3.95	19.45	2.30	2221.92
	27-2-D	579.38	331.77	74.18	332.89	57.91	12.61	71.77	9.81	62.21	769.59	13.70	35.19	4.02	20.23	2.42	2377.67
	27-2-E	461.59	289.49	70.17	329.06	60.44	14.20	76.04	10.16	64.26	743.24	13.89	34.81	3.69	17.93	2.04	2191.01
LFC-7 (granular francolite)	7-1-A	435.59	240.51	63.20	279.24	50.91	11.76	59.91	8.38	50.60	577.35	10.80	27.54	3.16	15.94	1.92	1836.83
	7-1-B	430.38	237.80	64.95	289.01	53.88	11.65	64.14	8.71	54.07	596.63	11.33	28.54	3.24	16.07	1.88	1872.27
	7-1-C	450.07	248.29	67.70	304.37	55.71	12.49	66.03	8.93	55.73	622.15	11.72	29.40	3.32	16.75	2.01	1954.66
	7-1-D	449.98	239.44	63.76	279.66	50.70	11.15	60.49	8.24	50.66	582.41	10.84	27.39	3.21	16.51	2.01	1856.43
	7-1-E	479.16	255.74	67.74	303.30	53.83	11.82	63.52	8.73	53.10	609.74	11.42	29.00	3.23	16.81	2.00	1969.15
	7-1-F	463.53	245.25	63.79	282.84	50.44	10.63	59.62	8.14	50.67	585.96	10.88	27.71	3.21	16.32	1.98	1880.96
	7-1-G	367.18	211.82	57.44	261.82	48.22	10.57	57.24	7.75	47.62	517.86	9.84	24.92	2.67	13.71	1.57	1640.23
	7-1-H	430.77	233.10	63.68	281.89	51.25	11.12	60.92	8.17	49.90	571.23	10.70	26.91	3.00	15.16	1.79	1819.61
LFC-7 (bioclastic francolite)	7-2-A	461.81	244.44	64.29	280.86	49.06	10.27	57.92	7.83	49.16	566.30	10.36	26.51	3.11	16.33	1.95	1850.18
	7-2-B	454.33	242.67	63.10	276.02	49.08	10.17	56.75	7.78	47.94	547.58	10.11	25.91	3.00	15.16	1.91	1811.51
	7-3-A	400.15	215.28	57.55	255.44	45.43	9.93	55.03	7.28	44.47	520.01	9.59	24.49	2.77	14.51	1.72	1663.64
	7-3-B	406.00	216.94	58.36	260.88	46.41	10.15	55.99	7.40	46.39	527.57	9.81	25.27	2.78	14.50	1.75	1690.20
	7-3-C	427.52	236.56	63.82	287.34	52.17	11.60	62.20	8.24	51.83	583.55	10.68	27.59	3.12	16.23	1.91	1844.38
	7-3-D	389.10	214.91	58.21	261.15	47.23	10.36	56.49	7.63	47.07	528.32	10.03	25.56	2.85	14.49	1.69	1675.11
	7-3-E	439.14	236.38	62.30	279.47	49.35	10.79	59.01	7.95	48.56	559.81	10.39	26.39	3.02	15.51	1.93	1810.00
	7-3-F	450.62	235.96	61.06	268.51	47.84	9.84	56.34	7.55	47.68	547.26	10.09	25.82	2.97	15.52	1.90	1788.98
	7-3-G	451.51	238.05	61.63	273.87	47.87	10.15	57.62	7.76	48.62	555.55	10.32	26.31	3.01	16.01	1.90	1810.20
	7-3-H	474.91	247.49	65.01	287.07	50.70	11.09	59.86	8.05	50.45	577.44	10.71	27.70	3.16	16.88	2.06	1892.57
	7-3-I	485.17	262.56	73.24	326.61	59.93	12.76	68.73	9.41	57.63	633.24	12.22	30.07	3.39	17.00	2.02	2053.98
	7-3-J	499.20	264.95	69.30	307.96	55.54	11.81	64.44	8.67	52.22	609.19	11.39	28.68	3.28	17.01	2.08	2005.72

Table 3. *Cont.*

Sample (Type)	Spot	La	Ce	Pr	Nd	Sm	Eu	Gd	Tb	Dy	Y	Ho	Er	Tm	Yb	Lu	ΣREY
	D6-1-1	18.39	9.94	2.41	9.81	1.46	0.28	2.24	0.35	2.96	39.23	0.86	2.34	0.40	2.92	0.40	93.98
	D6-1-3	10.18	6.34	1.61	6.46	1.09	0.23	1.59	0.24	2.56	29.67	0.64	1.68	0.33	1.69	0.27	64.59
	D6-1-5	13.65	7.71	1.96	8.31	1.94	0.30	2.24	0.43	3.25	41.00	0.85	2.85	0.44	3.47	0.48	88.88
	D6-1-6	11.44	6.40	1.62	6.48	1.45	0.24	1.74	0.29	2.48	31.91	0.67	1.91	0.30	1.98	0.30	69.22
LFC-6	D6-1-8	20.70	11.00	2.41	9.84	1.57	0.32	2.10	0.39	2.81	37.79	0.72	2.30	0.35	2.07	0.30	94.66
(dolomite)	D6-2-1	14.02	7.68	1.96	7.68	1.33	0.30	1.91	0.31	2.46	32.07	0.59	2.00	0.32	2.16	0.34	75.14
	D6-2-2	10.53	5.90	1.62	6.82	1.23	0.28	1.58	0.26	2.26	26.95	0.56	1.77	0.27	1.77	0.28	62.07
	D6-2-3	6.04	3.64	1.02	3.89	0.85	0.17	1.18	0.23	1.64	21.65	0.44	1.45	0.23	1.56	0.22	44.20
	D6-2-4	9.08	4.74	1.10	4.35	0.85	0.21	1.07	0.20	1.74	22.10	0.45	1.54	0.24	1.72	0.25	49.65
	D6-4-2	18.4	9.6	2.47	10.6	1.83	0.40	2.27	0.37	2.69	35.3	0.67	2.21	0.33	2.35	0.33	89.86

5. Discussion

5.1. Occurrence of REY

Phosphatic rocks have been reported to contain high ΣREY all over the word [1,37]. Previous research suggested that the REY in the Zhijin phosphorite were dominantly hosted in francolite by isomorphic substitution [14–19,22], while very small amounts of REY were adsorbed in francolite [15,17,38] or occurred as independent REY minerals [14,15]. Generally, REY are substituted into apatite via two dominant schemes: $REY^{3+} + Na^+ \leftrightarrow 2Ca^{2+}$ and/or $REY^{3+} + Si^{4+} \leftrightarrow Ca^{2+} + P^{5+}$ [39,40]. In our study, the ΣREY has a significantly positive correlation with P_2O_5, CaO, and F, which are the main components of francolite, indicating that REY are mainly enriched in the francolite. This is further supported by the results of in situ ΣREY analyses and can be observed from the element content mapping (Figure 6) that the rare earth elements are homogeneously distributed in the francolite particles.
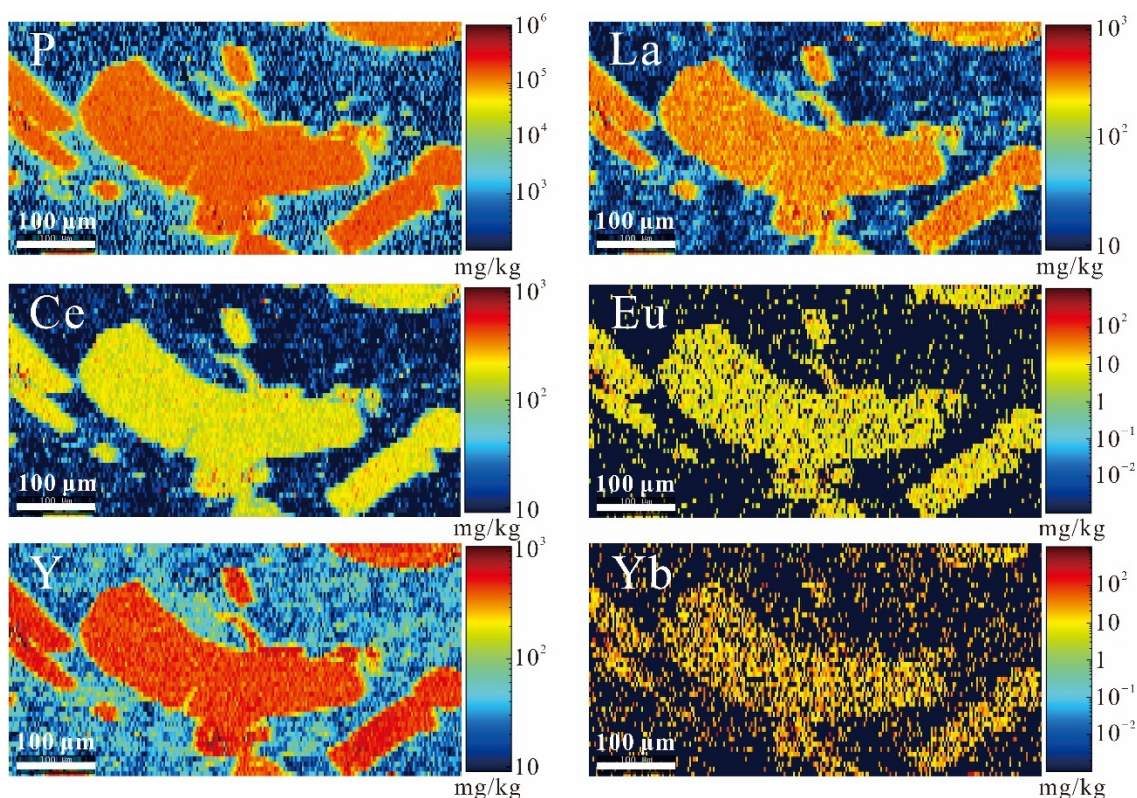
Figure 6. REY mapping of francolite grain from the LFC section.

5.2. REY Pattern

The PAAS-normalized REY pattern in phosphorites can be an important indicator for the depositional conditions and diagenetic effects, as well as REY sources [31,33,41,42]. The PAAS-normalized REY patterns of phosphate rocks and nodules studied by many researchers can be concluded as being seawater-like and "hat-shaped" [1,31,41,43]. Commonly, a seawater-like pattern is characterized by a negative Ce anomaly, HREE enrichment, as well as Y enrichment [44–48], whereas a hat-shaped pattern is distinguished by MREE enrichment and HREE depletion [31,41].

MREE enrichment is most common in phosphate rocks and sediments [24,43,49–56]. In this study, the REY pattern of whole rock analyses of four sections and that of francolite is quite similar (Figures 7 and 8), showing a typical hat-shaped pattern with MREE enrichment. Most studies have attributed this hat-shaped REY pattern in phosphate rocks to diagenetic conditions [33,43,48,55,57]. The MREE enrichment has been observed in authigenic phosphate that precipitates during early diagenesis [58,59], but there is also evidence that the timing of the uptake of MREEs occurs throughout early and late dia-

genesis [43]. During the diagenetic recrystallization of apatite, the MREEs preferentially substitute Ca^{2+} due to the similarity between the ionic radii of Ca and MREE [29,31]. The MREE enrichment has also been attributed to the preferential adsorption of MREE into organisms [60,61]. Research on the Ediacaran Weng'an phosphorite deposit indicates that biogenetic phosphorite might play a role in MREE enrichment [22,53]. However, in our case, bioclastic and granular francolite are both characterized by MREE enrichment, and the two types of francolite from the lower layer of the LFC section do not show significant differences in ΣREY. Thus, we propose that biological activity may not play an important role in REY enrichment in the Zhijin deposit.
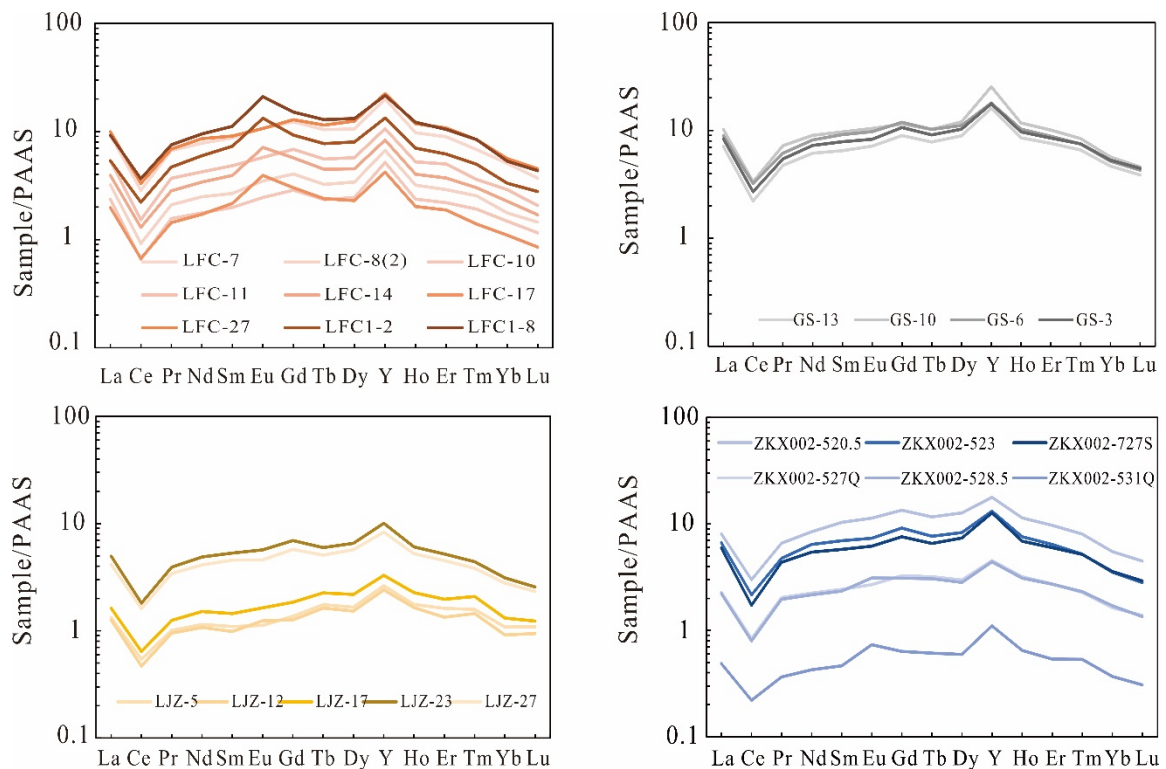
Figure 7. PAAS–normalized rare earth element distributions of phosphorites from four sections in Zhijin region.

It is believed that the REY pattern of seawater can be well preserved in carbonate sediments and rocks [62]. Therefore, the pattern of dolomites in this study can represent the seawater pattern at that time to a large extent. In Figure 8, we compare the REY patterns of different systems, and we propose that the REY patterns of dolomite from the LFC section are similar to that of modern seawater, whereas the REY pattern of francolite varies from seawater by a distinct HREE depletion, which can be the result of hydrothermal influence or diagenetic processes [33].
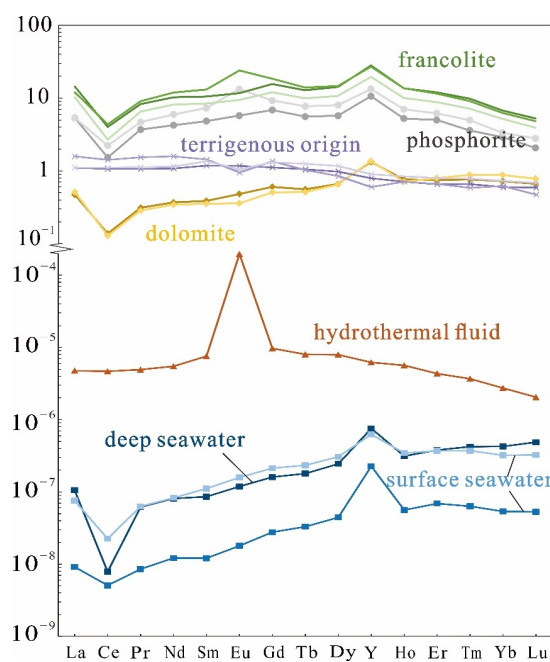
Figure 8. PAAS–normalized rare earth element distributions of different systems and samples. Data are based on reported REY, including high-temperature hydrothermal fluid [63], modern seawater from Indian Ocean and South Pacific Ocean [45,47] and terrigenous components [64]. Data of phosphorites and francolite and dolomite grains are from the LFC section, Zhijin deposit.

5.3. Redox Conditions

5.3.1. Ce Anomaly

A Ce anomaly in phosphate rocks is usually used as an effective indicator of redox conditions of the depositional environment during early diagenesis [52,65]. Commonly, a negative Ce anomaly can be a result of the oxidation of Ce^{3+} to Ce^{4+}, and this process occurs under oxic seawater conditions. Ce^{4+} is scavenged by Fe-Mn oxyhydroxides and organic matter, thus leaving the seawater depleted of Ce [56,66]. Therefore, sediments precipitating from oxic seawater record a negative anomaly and indicate an oxidizing environment [42,65]. In this study, the Ce/Ce* of phosphorites and francolite ranges from 0.32 to 0.52, as for many phosphorites [19,22,31,65], showing a distinct negative Ce anomaly. Since the high concentration of La can lead to great uncertainty in Ce/Ce* calculation [33], we use the method of Bau and Dulski (1996) to measure the La effect on Ce anomaly values (Figure 9a). In our study, all samples of phosphorites and francolite are plotted on the Pr/Pr*-Ce/Ce* diagram, which is divided into five domains. Figure 9a shows that samples from this study lie within the field IIIb, indicating real Ce anomalies of all the samples. Therefore, the negative Ce anomaly suggests oxic conditions during the deposition of the Zhijin phosphorites, which is supported by the Mo isotope data [25]. In the LFC section, the average Ce/Ce* of rocks from the lower layer is 0.37, and that of the upper layer is 0.42, implying that the degree of oxygenation decreased from the bottom to the top of the LFC section.

However, Ce/Ce* can also be affected by diagenetic processes, pH, and water depth [33,67]. Diagenetic processes will lead to REE enrichment and a decrease in $(Dy/Sm)_N$, and therefore the correlation between $\Sigma REY - Ce/Ce^*$ and $(Dy/Sm)_N - Ce/Ce^*$ can be used as a geochemical parameter to determine the effect of diagenetic processes [33,68]. Our data of Ce/Ce* from phosphorites and francolite do not show an obvious positive correlation with ΣREY (Figure 9b) or negative correlation with $(Dy/Sm)_N$ (Figure 9c), indicating that diagenetic processes did not significantly affect the Ce concentrations of phosphorite and francolite. However, we do not exclude the influence of pH and water depth. However, it should be noted that a Ce anomaly cannot alone determine the redox conditions.
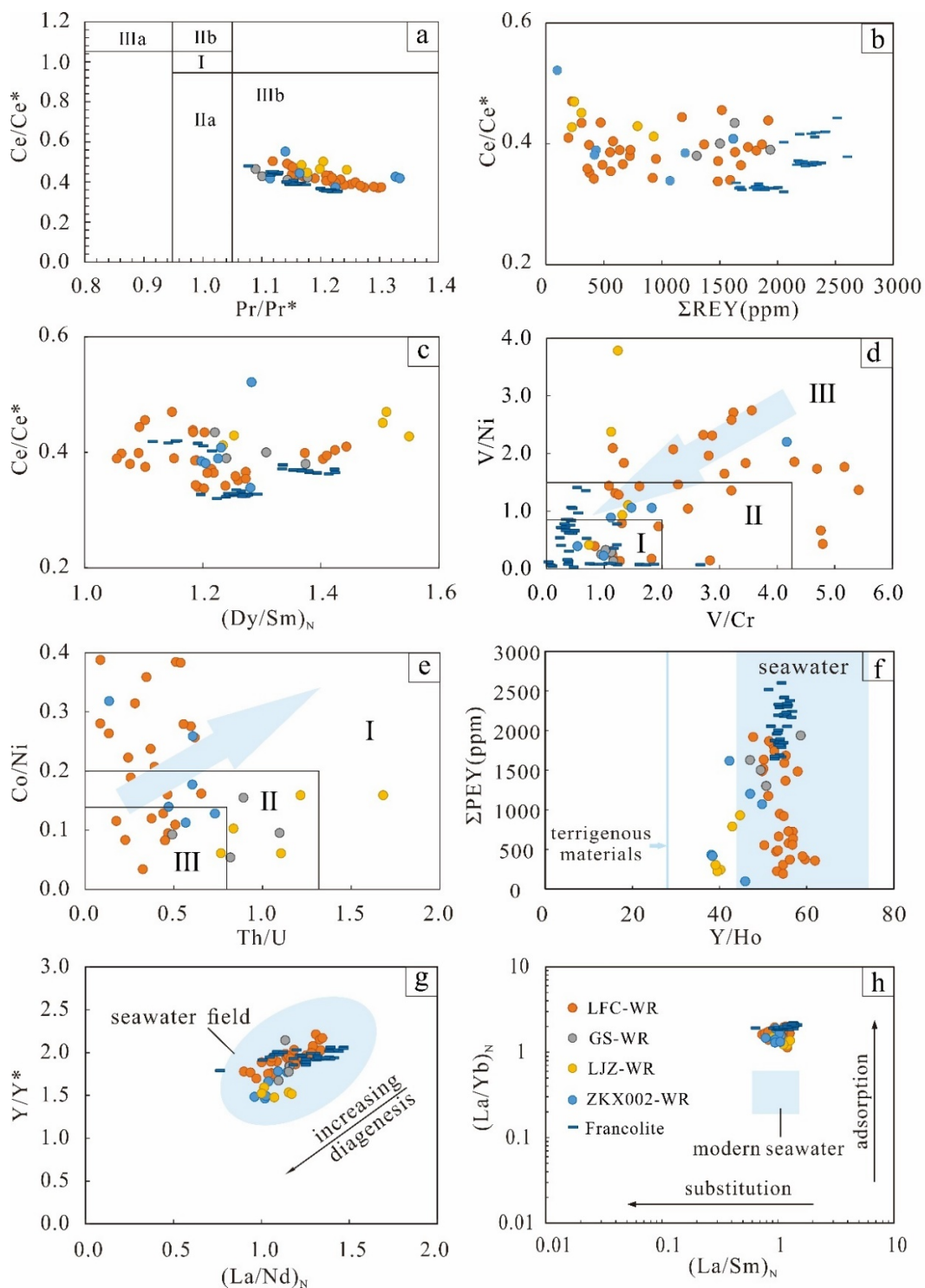
Figure 9. REE plots: (**a**) position of the data points in bivariate plot of Pr/Pr*-Ce/Ce*, modified after Bau and Dulski, 1996 [69]. The five fields are defined as follows: I: no La and Ce anomaly; IIa: positive La anomaly and no Ce anomaly; IIb: negative La anomaly and no Ce anomaly; IIIa: positive Ce anomaly; IIIb: negative Ce anomaly. (**b**) Ce/Ce*-ΣREY diagram based on Morad and Felitsyn (2001) [68] and Shields and Stille (2001) [33]. (**c**) Ce/Ce*– Dy_N/Sm_N diagram based on Morad and Felitsyn (2001) and Shields and Stille (2001). (**d**,**e**) V/Cr-V/Ni and Th/U-Co/Ni diagram of phosphorite and francolite samples from Zhijin deposit. Modified after Ross and Bustin (2006) [70] and Zhang et al. (2021) [29]. Legend: I: oxic environment, II: suboxic environment, III: anoxic environment. The arrow indicates the direction of oxic environment. (**f**) Y/Ho ratios of samples of

Zhijin phosphorites. The blue area represents the Y/Ho range of seawater [69], from 44 to 74. The blue line represents the Y/Ho ratio of terrigenous materials [71], which is 28. (**g**) La_N/Nd_N vs. Y/Y^* showing increasing diagenetic alteration with lowering Y/Y^* and La_N/Nd_N values, and (**h**) La_N/Sm_N vs. La_N/Yb_N showing increasing LREE concentrations during post-depositional porewater-rock interaction. Modified after Lumiste et al. (2019) [56] and Reynard et al. (1999) [57]. LFC-WR, GS-WR, LJZ-WR, and ZKX002-WR are whole rock samples from the four sections in Zhijin. LFC-Francolite is francolite from the LFC section, Zhijin region.

5.3.2. Eu Anomaly

A positive Eu anomaly is normally interpreted as a tracer for a reducing and anoxic depositional environment [50], or can represent a characteristic inherited from Eu-rich feldspar [33]. An Eu anomaly can also be influenced by hydrothermal fluids [24], as well as pH and temperature [72]. In this study, the Eu/Eu^* of phosphorites and francolite ranges from 0.88 to 1.82, showing negative to positive Eu anomalies. In the LFC section, although the average Eu/Eu^* of rocks from the lower layer (average = 1.21) is lower than that of the upper layer (average = 1.31), there is no continuous increase in Eu/Eu^* throughout the section. In contrast, the values of the Eu/Eu^* fluctuate around 1 (Tables S1 and S2). Fe isotope data indicate fluctuating oxic–suboxic seawater conditions during the deposition of Zhijin phosphorites, and suggest that these fluctuating conditions promoted Fe redox cycling, which caused the enrichment of REY [27].

Previous studies have proposed that Eu^{3+} could transfer to Eu^{2+} only under extremely reducing conditions [53,73,74]. However, in the Zhijin deposit, the Ce anomaly and Fe and Mo isotopes indicate oxic or suboxic-oxic conditions [25,27]. Thus, the positive Eu anomaly may indicate the effects of hydrothermal activity. Hydrothermal fluids can have a significant effect on the distribution of REY and REY minerals in phosphorites [51]. In the Zhijin deposit, the observation of hydrothermal veins, hydrothermal minerals and hydrothermally transformed minerals proved the existence of later hydrothermal activity [30]. Research also indicates that the Zhijin phosphorite formed in an anoxic hydrothermal sedimentary environment [29], indicating the influence of hydrothermal fluids.

5.3.3. Redox Sensitive Elements (RSEs)

The solubility of RSEs changes correspondingly under different redox conditions, resulting in their migration to water or sediment under different conditions. Thus, the content and ratios of these elements can be used to measure the redox conditions of sediments and rocks [75]. V/Ni, V/Cr, Th/U, and Co/Ni can be used as indicators to determine the redox state of paleo-marine environments [75]. In this study, we chose V, Ni, Cr, Co, Th, and U to determine the sedimentary conditions of the Zhijin deposits.

V is preferentially enriched in sediments in anoxic or near-anoxic water conditions compared with Ni and Cr [76,77]. Jones and Manning (1994) suggested that V/Cr < 2 indicates an oxic condition, and 2 < V/Cr < 4.25 indicates an anoxic condition [77]. Furthermore, the depositional environment can be divided into four types based on V/Ni ratios: an oxidation environment (V/Ni < 0.8), an oxygen-lean environment (0.8 < V/Ni < 1.5), an anoxic environment (1.5 < V/Ni < 6), and a sulfidic environment (V/Ni > 6) [29,76,78]. The V/Cr ratios of the Zhijin phosphorites and francolite are 0.54–13.4 and 0.03–2.67, respectively. The V/Ni ratios are 0.14–4.48 for phosphorites and 0.04–1.41 for francolite. In the V/Cr–V/Ni discriminant figures (Figure 9d), phosphorite and francolite data scatter in three regions, indicating fluctuating conditions.

U exists in the form of soluble U^{6+} under oxic conditions, and is reduced to insoluble U^{4+} in the reduced condition. Th appears as insoluble Th^{4+} under oxic conditions [79]. Therefore, the Th/U ratio is higher under oxic conditions, because U is released from sediment to seawater [79]. Jones and Manning (1994) suggested that Th/U > 1.33 indicates an oxidizing environment, 0.8 < Th/U < 1.33 indicates an oxygen-poor environment, and Th/U < 0.8 indicates an anoxic environment [77]. In a reducing environment, Ni moves to the sediments from organic matter, and the Co/Ni ratio in the sediments decreases [77].

Jones and Manning (1994) proposed that Co/Ni > 0.2 indicates an oxidized environment and a ratio < 0.14 indicates an anoxic environment [77]. The Th/U ratios of the Zhijin phosphorites range from 0.05 to 1.68, and the Co/Ni ratios are 0.06–1.58. In a Th/U–Co/Ni diagram (Figure 9e), phosphorites fall into the anoxic, suboxic, and oxic region, again indicating fluctuating redox conditions.

5.4. The Origin of the REY

5.4.1. The Sources of REY

Seawater, organic matter, terrigenous detrital minerals as well as hydrothermal fluids are considered as potential sources for REE in sedimentary phosphatic rocks [5,18,24,28,31]. Modern seawater is distinguished by a distinct negative Ce anomaly and relative enrichment of the HREE, especially Y enrichment, as well as positive La anomalies and high Y/Ho ratios [46,48,69]. However, there is a debate about whether the REY composition of seawater has changed over geological time. Though some researchers think the composition has changed, most researchers propose that seawater REY patterns have hardly changed throughout time, and the deviations from the modern recordings for bioapatite are considered the product of post-depositional REY exchange with pore water [33,43,48]. Carbonate has the potential for recording information of ambient seawater during deposition [71,80]. As we have discussed in Section 5.2, in our study, dolomite, the cement mineral of francolite, shows a similar REY pattern to modern seawater (Figure 8). The Ce anomalies in our samples have not been affected by diagenetic processes, indicating that the Ce anomaly represents the primary information regarding deposition. Though the REY pattern of francolite shows a different pattern than the dolomite and modern seawater, it preserves the characteristics of the negative Ce anomaly, which is the same as modern seawater, indicating the contribution of seawater.

Y and Ho are considered as geochemical twin elements that share similar valence and almost the same radii. Therefore, they behave similarly in most geological processes, and so the Y/Ho ratio is usually a constant in stable sedimentary rocks and minerals [46,81,82]. However, it differs in different systems due to the influence of these sedimentary environments or sources [69]. Because of the higher affinity of Ho towards Fe-Mn oxyhydroxides, the Y/Ho ratio in seawater is higher than that in chondritic materials and igneous rocks of 28 [44,56]. The Y/Ho ratio of modern seawater is 44~74 [82]. The Y/Ho ratio of terrigenous materials is approximately 28 [31], and hydrogenetic marine ferromanganese crust displays even lower Y/Ho, with a value of 17–25 [69]. In this study, the Y/Ho ratios of bulk rock and francolite samples from the LFC section are relatively concentrated (50–60) and indicate a seawater origin (Figure 9f). However, the values of the other three sections vary from 38.13 to 58.63 (mean of 44.92), which are lower than that of the LFC section (Figure 9f). Therefore, the lower Y/Ho of these sections (especially the LJZ and ZKX002 sections) indicate a possible origin of terrigenous materials, whereas the slight variation in the trend of the terrigenous materials suggests that a terrigenous effect does not play an important role in REY contribution. The detrital materials can also give rise to great enrichment of Nd, resulting in a Er/Nd value less than 0.1 [67,83]. In modern seawater, the value of the Er/Nd ratio is approximately 0.27 [84]. In this study, the value of the Er/Nd ratio in the studied phosphatic rocks ranges from 0.08 to 0.13, with an average of 0.10, which is lower than the value of seawater. Therefore, these ratio values may support a terrigenous origin of some of the REY [31]. However, diagenetic processes have an effect on the Er/Nd ratio [83], and a low Er/Nd can be a result of diagenetic processes.

The Y anomaly and La_N/Nd_N ratio are considered useful indicators for determining the post-depositional changes related to variations in the composition of circulating fluids [85]. These two parameters have positive anomalies in modern seawater [44,86]. Although they are not affected by environmental redox changes, diagenetic processes can have great influence on them [33]. In modern seawater, the Y anomaly varies between 1.5 and 2.3, and the La_N/Nd_N ratio is between 0.8 and 1.3 [33]. In our study, the Y anomaly in Zhijin phosphorites and francolite ranges from 1.46 to 2.21, and the La_N/Nd_N is from 0.76

to 1.47, both of which are similar to the seawater values (Figure 9g), indicating the samples were not significantly chemically affected by diagenesis. According to Shields and Stille, 2001, the Y anomaly and La_N/Nd_N ratios are expected to decrease during diagenesis [33]. In all of the samples from the Zhijin region, samples from the GS section, the LJZ section, and the ZKX002 section trend towards increasing diagenesis compared to those from the LFC section. This indicates that these three sections may have undergone relatively more intense diagenesis [33,85] (Figure 9g).

Reynard et al. (1999) suggested that the La_N/Yb_N ratio is affected by the substitution mechanism, whereas the La_N/Sm_N ratio is affected by adsorption, which often occurs in early diagenesis. As a result, the La_N/Sm_N ratio will increase if the REY uptake is governed by the adsorption mechanism and the La_N/Sm_N ratio will increase if adsorption dominates [57]. The La_N/Sm_N and La_N/Yb_N ratios of Zhijin phosphorites and francolite are 0.64–1.47 and 1.14–2.21, respectively. Compared to the seawater ratios, 0.6–1.6 for La/Sm and 0.2–0.5 for La_N/Yb_N [57], Zhijin phosphorites have a similar La_N/Sm_N ratio and a higher La_N/Yb_N ratio (Figure 9h). This suggests that adsorption dominates the REY uptake during early diagenesis near the water–sediment interface [56,57].

Furthermore, the seawater origin is demonstrated by the Ce/Ce* and Eu/Eu* (Figure 10). In Figure 10, whole rock and francolite samples from this study have been compared with different sources, including fossils, fish debris, iron oxide apatite (IOA)-type ore, hydrothermal, as well as seawater and deep-sea mud. In recent years, deep-sea muds were found to be enriched in REY, which are considered to be derived from seawater, pore water, Fe-Mn oxyhydroxides, and organic matter [39,56]. Research into the REE-rich deep-sea mud from the Minami-Torishima area, southeastern Japan, proposed that the REY pattern of bio-apatite in deep sea clay is influenced by the seawater [87]. In our case, we found the data of our samples to be plotted in a similar area to the mud apatite, around the area of seawater (Figure 10), implying the significant influence of seawater, consistent with the Y anomaly and La/Nd ratio. However, hydrothermal activity may have an effect on the REY data in Figure 10, deviating from the seawater region slightly towards the hydrothermal region. Furthermore, in our case, most of the francolite grains and phosphorites show Eu/Eu* values close to one (Figure 10, Tables S1 and S2), indicating the limited influence of hydrothermal activities during francolite formation.
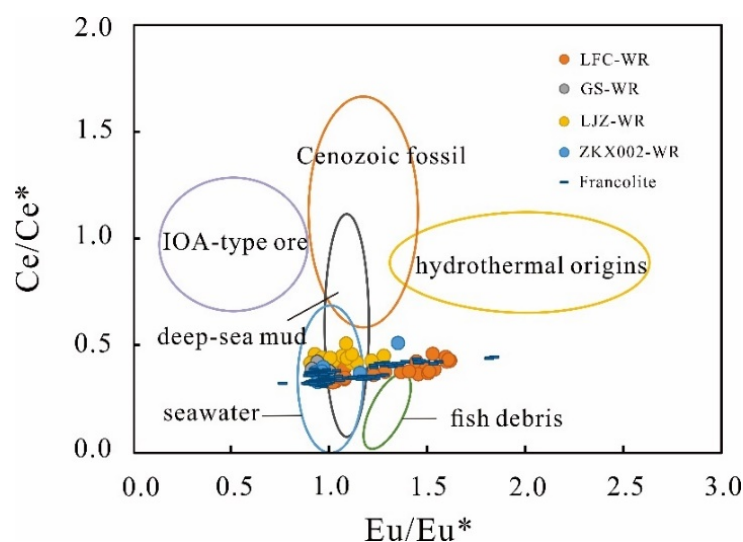

Figure 10. Ce and Eu anomalies of various sources of apatite. The involved REY were normalized by PAAS and were calculated as follows: $[Ce/Ce^*]_N = Ce_N/(La_N^{1/2} \times Pr_N^{1/2})$, $[Eu/Eu^*]_N = Eu_N/(Sm_N^{1/2} \times Gd_N^{1/2})$. For the data of Cenozoic fossils, REY were calculated as $[Ce/Ce^*]_N = Ce_N/(La_N^{2/3} \times Nd_N^{1/3})$, $[Eu/Eu^*]_N = Eu_N/(Sm_N^{2/3} \times Tb_N^{1/3})$. The data are from reported REY, including: Cenozoic fossils [54], apatite in deep-sea mud from the Pacific Ocean [8], seawater from the Pacific and the Atlantic Oceans [72], fish debris [88], apatite from IOA (iron oxide apatite)-type

ore deposit [89,90], and hydrothermal origin apatite [91,92]. LFC-WR, GS-WR, LJZ-WR, and ZKX002-WR are whole rock samples from the four sections in the Zhijin region. Francolite is francolite from the LFC section, Zhijin region.

5.4.2. The Enrichment Process of REY

During the early Cambrian, the breakup of the Rodinia supercontinent [93,94] and higher temperature [25] increased terrigenous weathering input, along with upwelling, providing P and REY in shallow seawater. At that time, the seawater became entirely oxic [25,26,95] and primary francolite precipitated by absorbing P and REY in this oxic seawater setting [53]. Fe-Mn oxyhydroxides adsorbed REY in seawater and then released them in a suboxic to anoxic environment [22]. Driven by the influence of increasingly intense ocean currents and sea waves, the primary francolite was abraded and transported to a constrained basin [22,29], and in this transportation process, francolite took on different shapes due to different transportation distances. In the constrained basin, the turbulent water created a fluctuating redox condition, promoting Fe redox cycling, resulting in a great enrichment of REY in porewater and then in francolite [27]. Additionally, the diagenesis might have an effect on the enrichment of MREE [43,55]. The REY uptake occurred during the primary sedimentary stage, transportation stage and early diagenesis [22,27,58,59]. Hydrothermal activity may have affected the REY content, but not to a large degree [29,30].

6. Conclusions

1. The REY in the Zhijin deposit are mainly contained in francolite. The phosphorites and francolite show a hat-shaped pattern characterized by MREE enrichment and HREE depletion, indicating the influence of diagenetic processes.
2. Ce anomalies indicate a primary oxic sedimentation condition. The Eu anomalies and RSEs indicate fluctuating depositional conditions during diagenesis, which can promote the enrichment of REY.
3. We propose that the main origin of REY in the Zhijin phosphorites is seawater, though terrigenous materials may have a minor contribution. The REY were absorbed by francolite during primary sedimentation, transportation, and early diagenesis. Hydrothermal fluids have a minor influence on REY concentrations.

Supplementary Materials: The following supporting information can be downloaded at: https://www.mdpi.com/article/10.3390/min12040408/s1, Table S1: REY ratios and selected trace element of phosphorites and phosphatic dolomites (contents of elements are in ppm); Table S2: REY ratios and selected trace element of francolite and dolomite grains (contents of elements are in ppm, "-" means not detected). Table S3: Selected major elements of francolite from the LFC section (%, "-" means not detected).

Author Contributions: Conceptualization: S.H. and Y.X.; formal analysis, S.H.; investigation, S.H., Y.X., J.X., Z.X., H.G., S.W. and X.G.; writing—original draft, S.H.; writing—review and editing, Y.X., D.G., Z.X., Q.T. and H.Y. All authors have read and agreed to the published version of the manuscript.

Data Availability Statement: All data generated or used during the study appear in the submitted article and supplementary materials.

Conflicts of Interest: The authors declare no conflict of interest.

References

1. Emsbo, P.; McLaughlin, P.I.; Breit, G.N.; du Bray, E.A.; Koenig, A.E. Rare earth elements in sedimentary phosphate deposits: Solution to the global REE crisis? *Gondwana Res.* **2015**, *27*, 776–785. [CrossRef]
2. Dushyantha, N.; Batapola, N.; Ilankoon, I.M.S.K.; Rohitha, S.; Premasiri, R.; Abeysinghe, B.; Ratnayake, N.; Dissanayake, K. The story of rare earth elements (REEs): Occurrences, global distribution, genesis, geology, mineralogy and global production. *Ore Geol. Rev.* **2020**, *122*, 103521. [CrossRef]

3. Hein, J.; Koschinsky, A.; Mikesell, M.; Mizell, K.; Glenn, C.; Wood, R. Marine Phosphorites as Potential Resources for Heavy Rare Earth Elements and Yttrium. *Minerals* **2016**, *6*, 88. [CrossRef]

4. Jiang, X.; Feng, L. Comprehensive utilization of associated rare earth element resources in phosphate rocks. *China Popul. Resour. Environ.* **2011**, *21*, 195–199. (In Chinese with English Abstract)

5. Fakhry, A.A.; Eid, K.A.; Mahdy, A.A. Distribution of REE in shales overlying the Abu Tartur phosphorite deposit, western desert, Egypt. *J. Alloys Compd.* **1998**, *275*, 929–933. [CrossRef]

6. Awadalla, G.S. Geochemistry and microprobe investigations of Abu Tartur REE-bearing phosphorite, Western Desert, Egypt. *J. Afr. Earth Sci.* **2010**, *57*, 431–443. [CrossRef]

7. Tanaka, E.; Nakamura, K.; Yasukawa, K.; Mimura, K.; Fujinaga, K.; Iijima, K.; Nozaki, T.; Kato, Y. Chemostratigraphy of deep-sea sediments in the western North Pacific Ocean: Implications for genesis of mud highly enriched in rare-earth elements and yttrium. *Ore Geol. Rev.* **2020**, *119*, 103392. [CrossRef]

8. Kato, Y.; Fujinaga, K.; Nakamura, K.; Takaya, Y.; Kitamura, K.; Ohta, J.; Toda, R.; Nakashima, T.; Iwamori, H. Deep-sea mud in the Pacific Ocean as a potential resource for rare-earth elements. *Nat. Geosci.* **2011**, *4*, 535–539. [CrossRef]

9. Iijima, K.; Yasukawa, K.; Fujinaga, K.; Nakamura, K.; Machida, S.; Takaya, Y.; Ohta, J.; Haraguchi, S.; Nishio, Y.; Usui, Y.; et al. Discovery of extremely REY-rich mud in the western North Pacific Ocean. *Geochem. J.* **2016**, *50*, 557–573. [CrossRef]

10. Ye, L. *Phosphorites in China*; Science Press: Beijing, China, 1989. (In Chinese)

11. Meng, Q.T.; Lan, A.P.; Ye, C. *A Report on Integrated Exploration of Phosphorus (Rare Earth) Deposits in Zhijin Area, Guizhou Province*; Fourth Geological Brigade of Guizhou Geological and Mineral Exploration and Development Bureau: Guizhou, China, 2014. (In Chinese)

12. Yang, J.; He, T. Zhijin county Guizhou province Xinhua containing rare earth phosphate rock deposit geological characteristics and reasons discussed. *Geol. Chem. Miner.* **2013**, *35*, 27–33. (In Chinese with English Abstract)

13. Wang, J.; Zhang, J. Study on characteristics of material composition and ore REE of Zhijin dolomitic phosphorite. *China Non-Met. Min. Ind. Her.* **2011**, *87*, 25–59. (In Chinese with English Abstract)

14. Liu, S.; Hu, R.; Zhou, G.; Gong, G.; Jin, Z.; Zheng, W. Study on the mineral Composition of the clastic phosphate in Zhijin phosphate deposits, China. *Acta Mineral. Sin.* **2008**, *28*, 244–250. (In Chinese with English Abstract)

15. Zhang, Y.; Gong, M.; Li, H. Occurrence of REE in rare earth phosphorite in Zhijin area, Guizhou. *J. Earth Sci. Environ.* **2007**, *29*, 362–368. (In Chinese with English Abstract)

16. Xie, H.; Zhu, L. Existing state and distribution regularity of rare earth elements from early Cambrian phosphorite in Guizhou. *J. Chin. Soc. Rare Earths* **2012**, *30*, 620–627. (In Chinese with English Abstract)

17. Chen, J.; Zhang, J.; Yang, R. Mode of occurrence of rare earth elements in posphorite in Zhijin county, Guizhou province, China. *Acta Mineral. Sin.* **2010**, *30*, 123–129. (In Chinese with English Abstract)

18. Zhang, J.; Sun, C.; Gong, M.; Zhang, Q.; Chen, D.; Cheng, J. Geochemical characteristics and occurrence states of the REE elements of the phosphorite in Xinhua, Zhijin, Guizhou. *Chin. Rare Earths* **2007**, *28*, 75–79. (In Chinese with English Abstract)

19. Liu, X.Q.; Zhang, H.; Tang, Y.; Liu, Y.L. REE Geochemical Characteristic of Apatite: Implications for Ore Genesis of the Zhijin Phosphorite. *Minerals* **2020**, *10*, 1012.

20. Liu, J.; Wen, H.; Zhang, Y.; Fan, H.; Zhu, C. Mo isotopic signature of non euxinic sediments and its paleo oceanic significance. *Acta Mineral. Sin.* **2015**, *89*, 72–73. (In Chinese with English Abstract)

21. Liu, J.; Wen, H.; Liu, S.; Fan, H.; Zhang, Y. Structures and sedimentary environment of phosphorite in Zhijin county, Guizhou province, China. *Acta Mineral. Sin.* **2016**, *36*, 253–259. (In Chinese with English Abstract)

22. Yang, H.; Zhao, Z.; Xia, Y.; Xiao, J. REY enrichment mechanisms in the early Cambrian phosphorite from South China. *Sediment. Geol.* **2021**, *426*, 106041. [CrossRef]

23. Wang, M.; Sun, X.; Ma, M. Rare earth elements geochemistry and genesis of Xinhua large-size phosphorite deposit in western Guizhou. *Miner. Depos.* **2004**, *23*, 484–493. (In Chinese with English Abstract)

24. Guo, H.; Xia, Y.; He, S.; Xie, Z.; Wei, D.; Lei, B. Geochemical characteristics of Zhijin phosphorite type rare-earth deposit, Guizhou province, China. *Acta Mineral. Sin.* **2017**, *37*, 755–763. (In Chinese with English Abstract)

25. Yang, H.; Xiao, J.; Xia, Y.; Xie, Z.; Tan, Q.; Xu, J.; He, S.; Wu, S.; Liu, X.; Gong, X. Phosphorite generative processes around the Precambrian-Cambrian boundary in South China: An integrated study of Mo and phosphate O isotopic compositions. *Geosci. Front.* **2021**, *12*, 101187. [CrossRef]

26. Fan, H.; Wen, H.; Zhu, X. Marine redox conditions in the Early Cambrian ocean: Insights from the Lower Cambrian phosphorite deposits, South China. *J. Earth Sci.* **2016**, *27*, 282–296. [CrossRef]

27. Zhang, H.; Fan, H.; Wen, H.; Han, T.; Zhou, T.; Xia, Y. Controls of discrepant REY enrichment in the early Cambrian phosphorites. *Geochim. Cosmochim. Acta* **2022**, *324*, 117–139. [CrossRef]

28. Ilyin, A.V. Rare-earth geochemistry of 'old' phosphorites and probability of syngenetic precipitation and accumulation of phosphate. *Chem. Geol.* **1998**, *144*, 143–256. [CrossRef]

29. Zhang, Z.; Jiang, Y.; Niu, H.; Xing, J.; Yan, S.; Li, A.; Weng, Q.; Zhao, X. Enrichment of rare earth elements in the early Cambrian Zhijin phosphorite deposit, SW China: Evidence from francolite micro-petrography and geochemistry. *Ore Geol. Rev.* **2021**, *138*, 104342. [CrossRef]

30. Xing, J.Q.; Jiang, Y.H.; Xian, H.Y.; Zhang, Z.Y.; Yang, Y.P.; Tan, W.; Liang, X.L.; Niu, H.C.; He, H.P.; Zhu, J.X. Hydrothermal activity during the formation of REY-rich phosphorites in the early Cambrian Gezhongwu Formation, Zhijin, South China: A micro- and nano-scale mineralogical study. *Ore Geol. Rev.* **2021**, *136*, 104224. [CrossRef]

31. Abedini, A.; Calagari, A.A. REEs geochemical characteristics of lower Cambrian phosphatic rocks in the Gorgan-Rasht Zone, northern Iran: Implications for diagenetic effects and depositional conditions. *J. Afr. Earth Sci.* **2017**, *135*, 115–124. [CrossRef]

32. Guo, Q.; Shields, G.A.; Liu, C.; Strauss, H.; Zhu, M.; Pi, D.; Goldberg, T.; Yang, X. Trace element chemostratigraphy of two Ediacaran–Cambrian successions in South China: Implications for organosedimentary metal enrichment and silicification in the Early Cambrian. *Palaeogeogr. Palaeoclim. Palaeoecol.* **2007**, *254*, 194–216. [CrossRef]

33. Shields, G.; Stille, P. Diagenetic constraints on the use of cerium anomalies as palaeoseawater redox proxies: An isotopic and REE study of Cambrian phosphorites. *Chem. Geol.* **2001**, *175*, 29–48. [CrossRef]

34. Steiner, M.; Wallis, E.; Erdtmann, B.-D.; Zhao, Y.; Yang, R. Submarine-hydrothermal exhalative ore layers in black shales from South China and associated fossils Ð insights into a Lower Cambrian facies and bio-evolution. *Palaeogeogr. Palaeoclimatol. Palaeoecol.* **2001**, *169*, 191. [CrossRef]

35. Chew, D.M.; Babechuk, M.G.; Cogné, N.; Mark, C.; O'Sullivan, G.J.; Henrichs, I.A.; Doepke, D.; McKenna, C.A. (LA,Q)-ICPMS trace-element analyses of Durango and McClure Mountain apatite and implications for making natural LA-ICPMS mineral standards. *Chem. Geol.* **2016**, *435*, 35–48. [CrossRef]

36. Mao, T.; Yang, R. Micro-structural Characteristics and Composotion of the Small Shelly Fossils in Cambrian phosphorites, Zhijin, Guizhou. *Acta Micropalaeontol. Sin.* **2013**, *30*, 100–207.

37. Zhang, J.; Zhang, Q.; Chen, D. REE geochemistry of the Xinhua REE-bearing phosphorus deposit, Zhijin county, Guizhou province. *Geol. Prospect.* **2004**, *40*, 41–44. (In Chinese with English Abstract)

38. Duan, K.; Wang, D.; Xiong, X.; Lian, W.; Gao, P.; Wang, Y.; Zhang, Y. A review of a preliminary quantitative study and genetic analysis for rare earth elements of ionic adsorption state in phosphate ore deposit in Zhijin, Guizhou province. *Rock Miner. Anal.* **2014**, *33*, 118–125. (In Chinese with English Abstract)

39. Liao, J.; Sun, X.; Li, D.; Sa, R.; Lu, Y.; Lin, Z.; Xu, L.; Zhan, R.; Pan, Y.; Xu, H. New insights into nanostructure and geochemistry of bioapatite in REE-rich deep-sea sediments: LA-ICP-MS, TEM, and Z-contrast imaging studies. *Chem. Geol.* **2019**, *512*, 58–68. [CrossRef]

40. Hughes, J.M.; Rakovan, J.F. Structurally Robust, Chemically Diverse: Apatite and Apatite Supergroup Minerals. *Elements* **2015**, *11*, 165–170. [CrossRef]

41. Zhu, B.; Jiang, S.Y.; Yang, J.H.; Pi, D.H.; Ling, H.F.; Chen, Y.Q. Rare earth element and Sr-Nd isotope geochemistry of phosphate nodules from the lower Cambrian Niutitang Formation, NW Hunan Province, South China. *Palaeogeogr. Palaeoclim. Palaeoecol.* **2014**, *398*, 132–143. [CrossRef]

42. Garnit, H.; Bouhlel, S.; Barca, D.; Chtara, C. Application of LA-ICP-MS to sedimentary phosphatic particles from Tunisian phosphorite deposits: Insights from trace elements and REE into paleo-depositional environments. *Chem. Erde-Geochem.* **2012**, *72*, 127–139. [CrossRef]

43. Bright, C.A.; Cruse, A.M.; Lyons, T.W.; MacLeod, K.G.; Glascock, M.D.; Ethington, R.L. Seawater rare-earth element patterns preserved in apatite of Pennsylvanian conodonts? *Geochim. Cosmochim. Acta* **2009**, *73*, 1609–1624. [CrossRef]

44. Bau, M.; Dulski, P. Distribution of yttrium and rare-earth elements in the Penge and Kuruman iron-formations, Transvaal Supergroup, South Africa. *Precambrian Res.* **1996**, *79*, 37–55. [CrossRef]

45. Zhang, J.; Yoshiyuki, N. Rare earth elements and yttrium in seawater: ICP-MS determinations in the East Caroline, Coral Sea, and South Fiji basins of the western South Pacific Ocean. *Geochim. Cosmochim. Acta* **1996**, *60*, 4631–4644. [CrossRef]

46. Nozaki, Y.; Zhang, J.; Amakawa, H. The fractionation between Y and Ho in the marine environment. *Earth Planet. Sci. Lett.* **1997**, *148*, 329–340. [CrossRef]

47. Nozaki, Y.; Alibo, D.S. Importance of vertical geochemical processes in controlling the oceanic profiles of dissolved rare earth elements in the northeastern Indian Ocean. *Earth Planet. Sci. Lett.* **2003**, *205*, 155–172. [CrossRef]

48. Shields, G.A.; Webb, G.E. Has the REE composition of seawater changed over geological time? *Chem. Geol.* **2004**, *204*, 103–107. [CrossRef]

49. Stéphanie, P.; Christophe, L.; Jean-Pierre, G.; Gilles, D.; Sheppar, S.M.F. Rare earth element contents of Jurassic fish and reptile teeth and their potential relation to seawater composition (Anglo-Paris Basin, France and England. *Chem. Geol.* **2002**, *186*, 1–16.

50. Jiang, S.-Y.; Zhao, H.-X.; Chen, Y.-Q.; Yang, T.; Yang, J.-H.; Ling, H.-F. Trace and rare earth element geochemistry of phosphate nodules from the lower Cambrian black shale sequence in the Mufu Mountain of Nanjing, Jiangsu province, China. *Chem. Geol.* **2007**, *244*, 584–604. [CrossRef]

51. Pi, D.-H.; Liu, C.-Q.; Shields-Zhou, G.A.; Jiang, S.-Y. Trace and rare earth element geochemistry of black shale and kerogen in the early Cambrian Niutitang Formation in Guizhou province, South China: Constraints for redox environments and origin of metal enrichments. *Precambrian Res.* **2013**, *225*, 218–229. [CrossRef]

52. Xin, H.; Jiang, S.; Yang, J.; Wu, H.; Pi, D. Rare earth element geochemistry of phosphatic rocks in Neoproterozoic Ediacaran Doushantuo Formation in Hushan Section from the Yangtze Gorges Area, South China. *J. Earth Sci.* **2016**, *27*, 204–210. [CrossRef]

53. Yang, H.Y.; Xiao, J.F.; Xia, Y.; Xie, Z.J.; Tan, Q.P.; Xu, J.B.; Guo, H.Y.; He, S.; Wu, S.W. Origin of the Ediacaran Weng'an and Kaiyang phosphorite deposits in the Nanhua basin, SW China. *J. Asian Earth Sci.* **2019**, *182*, 103931. [CrossRef]

54. Laenen, B.; Hertogen, J.; Vandenberghe, N. The variation of the trace-element content of fossil biogenic apatite through eustatic sea-level cycles. *Palaeogeogr. Palaeoclim. Palaeoecol.* **1997**, *132*, 325–342. [CrossRef]
55. Trotter, J.A.; Eggins, S.M. Chemical systematics of conodont apatite determined by laser ablation ICPMS. *Chem. Geol.* **2006**, *233*, 196–216. [CrossRef]
56. Lumiste, K.; Mänd, K.; Bailey, J.; Paiste, P.; Lang, L.; Lepland, A.; Kirsimäe, K. REE+Y uptake and diagenesis in Recent sedimentary apatites. *Chem. Geol.* **2019**, *525*, 268–281. [CrossRef]
57. Reynard, B.; Lecuyer, C.; Grandjean, P. Crystal-chemical controls on rare-earth element concentrations in fossil biogenic apatites and implications for paleoenvironmental reconstructions. *Chem. Geol.* **1999**, *155*, 233–241. [CrossRef]
58. Byrne, R.H.; Liu, X.W.; Schijf, J. The influence of phosphate coprecipitation on rare earth distributions in natural waters. *Geochim. Cosmochim. Acta* **1996**, *60*, 3341–3346. [CrossRef]
59. Rasmussen, B.; Buick, R.; Taylor, W.R. Removal of oceanic REE by authigenic precipitation of phosphatic minerals. *Earth Planet. Sci. Lett.* **1998**, *164*, 135–149. [CrossRef]
60. Felitsyn, S.; Morad, S. REE patterns in latest Neoproterozoic–early Cambrian phosphate concretions and associated organic matter. *Chem. Geol.* **2002**, *187*, 257–265. [CrossRef]
61. Wright, J.; Schrader, H.; Holser, W.T. Paleoredox Variations in Ancient Oceans Recorded by Rare-Earth Elements in Fossil Apatite. *Geochim. Cosmochim. Acta* **1987**, *51*, 631–644. [CrossRef]
62. Tostevin, R.; Shields, G.A.; Tarbuck, G.M.; He, T.C.; Clarkson, M.O.; Wood, R.A. Effective use of cerium anomalies as a redox proxy in carbonate-dominated marine settings. *Chem. Geol.* **2016**, *438*, 146–162. [CrossRef]
63. Bau, M.; Dulski, P. Comparing yttrium and rare earths in hydrothermal fluids from the Mid-Atlantic Ridge implications for Y and REE behaviour during near-vent mixing and for the YrHo ratio of Proterozoic seawater. *Chem. Geol.* **1999**, *155*, 77–90. [CrossRef]
64. Lu, L.; Liu, Y.; Liu, H.; Zhao, Z.; Wang, C.; Xu, X. Geochemical and Geochronological Constraints on the Genesis of Ion-Adsorption-Type REE Mineralization in the Lincang Pluton, SW China. *Minerals* **2020**, *10*, 1116. [CrossRef]
65. Khan, S.A.; Khan, K.F.; Dar, S.A. REE geochemistry of Early Cambrian phosphorites of Masrana and Kimoi blocks, Uttarakhand, India. *Arab. J. Geosci.* **2016**, *9*, 456. [CrossRef]
66. Alibo, D.S.; Nozaki, Y. Rare earth elements in seawater: Particle association, shale-normalization, and Ce oxidation. *Geochim. Cosmochim. Acta* **1999**, *63*, 363–372. [CrossRef]
67. German, C.R.; Elderfield, H. Application of the Ce Anomaly as a Paleoredox Indicator: The Ground Rules. *Paleoceanography* **1990**, *5*, 823–833. [CrossRef]
68. Morad, S.; Felitsyn, S. Identification of primary Ce-anomaly signatures in fossil biogenic apatite: Implication for the Cambrian oceanic anoxia and phosphogenesis. *Sediment. Geol.* **2001**, *143*, 259–264. [CrossRef]
69. Bau, M. Controls on the fractionation of isovalent trace elements in magmatic and aqueous systems: Evidence from Y/Ho, Zr/Hf, and lanthanide tetrad effect. *Contrib. Mineral. Petrol.* **1996**, *123*, 323–333. [CrossRef]
70. Ross, D.J.K.; Bustin, R.M. Sediment geochemistry of the Lower Jurassic Gordondale Member, northeastern British Columbia. *Bull. Can. Pet. Geol.* **2006**, *54*, 337–365. [CrossRef]
71. Webb, G.E.; Kamber, B.S. Rare earth elements in Holocene reefal microbialites: A new shallow seawater proxy. *Geochim. Cosmochim. Acta* **2000**, *64*, 1557–1565. [CrossRef]
72. Debaar, H.J.W.; Bacon, M.P.; Brewer, P.G.; Bruland, K.W. Rare-Earth Elements in the Pacific and Atlantic Oceans. *Geochim. Cosmochim. Acta* **1985**, *49*, 1943–1959. [CrossRef]
73. Kidder, D.L.; Krishnaswamy, R.; Mapes, R.H. Elemental mobility in phosphatic shales during concretion growth and implications for provenance analysis. *Chem. Geol.* **2003**, *198*, 335–353. [CrossRef]
74. Yang, H.; Xiao, J.; Xia, Y.; Zhao, Z.; Xie, Z.; He, S.; Wu, S. Diagenesis of Ediacaran—early Cambrian phosphorite: Comparisons with recent phosphate sediments based on LA-ICP-MS and EMPA. *Ore Geol. Rev.* **2022**, *144*, 104813. [CrossRef]
75. Chang, H.; Chu, X.; Feng, L.-J.; Huang, J.; Zhang, Q. Redox Sensitive Trace Elements as Paleoenvironments Proxies. *Geol. Rev.* **2009**, *55*, 91–99.
76. Lewan, M.D.; Maynard, J.B. Factors Controlling Enrichment of Vanadium and Nickel in the Bitumen of Organic Sedimentary-Rocks. *Geochim. Cosmochim. Acta* **1982**, *46*, 2547–2560. [CrossRef]
77. Jones, B.; Manning, D.A.C. Comparison of Geochemical Indexes Used for the Interpretation of Palaeoredox Conditions in Ancient Mudstones. *Chem. Geol.* **1994**, *111*, 111–129. [CrossRef]
78. Lewan, M.D. Factors Controlling the Proportionality of Vanadium to Nickel in Crude Oils. *Geochim. Cosmochim. Acta* **1984**, *48*, 2231–2238. [CrossRef]
79. Kimura, H.; Watanabe, Y. Oceanic anoxia at the Precambrian-Cambrian boundary. *Geology* **2001**, *29*, 995–998. [CrossRef]
80. Xin, H.; Jiang, S.-Y.; Yang, J.-H.; Wu, H.-P.; Pi, D.-H. Rare earth element and Sr–Nd isotope geochemistry of phosphatic rocks in Neoproterozoic Ediacaran Doushantuo Formation in Zhangcunping section from western Hubei Province, South China. *Palaeogeogr. Palaeoclim. Palaeoecol.* **2015**, *440*, 712–724. [CrossRef]
81. Bau, M.; Dulski, P.; Moller, P. Yttrium and Holmium in South-Pacific Seawater—Vertical-Distribution and Possible Fractionation Mechanisms. *Chem. Erde-Geochem.* **1995**, *55*, 1–16.
82. Pack, A.; Russell, S.S.; Shelley, J.M.G.; van Zuilen, M. Geo- and cosmochemistry of the twin elements yttrium and holmium. *Geochim. Cosmochim. Acta* **2007**, *71*, 4592–4608. [CrossRef]

83. Bellanca, A.; Masetti, D.; Neri, R. Rare earth elements in limestone/marlstone couplets from the Albian-Cenomanian Cismon section (Venetian region, northern Italy): Assessing REE sensitivity to environmental changes. *Chem. Geol.* **1997**, *141*, 141–152. [CrossRef]

84. de Baar, H.J.W.; German, C.R.; Elderfield, H.; van Gaans, P. Rare earth element distributions in anoxic waters of the Cariaco Trench. *Geochim. Cosmochim. Acta* **1988**, *52*, 1203–1219. [CrossRef]

85. Fazio, A.M.; Scasso, R.A.; Castro, L.N.; Carey, S. Geochemistry of rare earth elements in early-diagenetic miocene phosphatic concretions of Patagonia, Argentina: Phosphogenetic implications. *Deep. Sea Res. Part II Top. Stud. Oceanogr.* **2007**, *54*, 1414–1432. [CrossRef]

86. Zhang, J.; Amakaw, H.; Nozak, Y. The comparative behaviors of Yttrium and Lanthanides in the seawater of the North Pacific. *Geophys. Res. Lett.* **1994**, *21*, 2677–2680. [CrossRef]

87. Kon, Y.; Hoshino, M.; Sanematsu, K.; Morita, S.; Tsunematsu, M.; Okamoto, N.; Yano, N.; Tanaka, M.; Takagi, T. Geochemical Characteristics of Apatite in Heavy REE-rich Deep-Sea Mud from Minami-Torishima Area, Southeastern Japan. *Resour. Geol.* **2014**, *64*, 47–57. [CrossRef]

88. Bernat, M. Les isotopes de l'uranium et du thorium et les terres rares dans l'environnement marin. *Cuh. ORSTOM Sér. GPol.* **1975**, *7*, 65–83.

89. Frietsch, R.; Perdahl, J.A. Rare-Earth Elements in Apatite and Magnetite in Kiruna-Type Iron-Ores and Some Other Iron-Ore Types. *Ore Geol. Rev.* **1995**, *9*, 489–510. [CrossRef]

90. Mokhtari, M.A.A.; Zadeh, G.H.; Emami, M.H. Genesis of iron-apatite ores in Posht-e-Badam Block (Central Iran) using REE geochemistry. *J. Earth Syst. Sci.* **2013**, *122*, 795–807. [CrossRef]

91. Stalder, M.; Rozendaal, A. Apatite nodules as an indicator of depositional environment and ore genesis for the Mesoproterozoic Broken Hill-type Gamsberg Zn?Pb deposit, Namaqua Province, South Africa. *Miner. Depos.* **2004**, *39*, 189–203. [CrossRef]

92. Halpin, K.M. *The Characteristics and Origin of the Hoidas Lake REE Deposit*; University of Saskatchewan Saskatoon: Saskatoon, SK, Canada, 2010.

93. Shields, G.A. A normalised seawater strontium isotope curve: Possible implications for Neoproterozoic-Cambrian weathering rates and the further oxygenation of the Earth. *eEarth* **2007**, *2*, 35–42. [CrossRef]

94. Halverson, G.P.; Wade, B.P.; Hurtgen, M.T.; Barovich, K.M. Neoproterozoic chemo stratigraphy. *Precambrian Res.* **2010**, *182*, 337–350. [CrossRef]

95. Goldberg, T.; Strauss, H.; Guo, Q.; Liu, C. Reconstructing marine redox conditions for the Early Cambrian Yangtze Platform: Evidence from biogenic sulphur and organic carbon isotopes. *Palaeogeogr. Palaeoclimatol. Palaeoecol.* **2007**, *254*, 175–193. [CrossRef]